

Gravitational form factors and mechanical properties of the nucleon in a meson dominance approach

Wojciech Broniowski^{1,2,*} and Enrique Ruiz Arriola^{3,†}

¹*H. Niewodniczański Institute of Nuclear Physics PAN, 31-342 Cracow, Poland*

²*Institute of Physics, Jan Kochanowski University, 25-406 Kielce, Poland*

³*Departamento de Física Atómica, Molecular y Nuclear and Instituto Carlos I de Física Teórica y Computacional, Universidad de Granada, E-18071 Granada, Spain*

(Dated: March 18, 2025)

We analyze the gravitational form factors and mechanical properties of the nucleon, focusing on both some general issues as well as on modeling with meson dominance. We show that the lattice QCD results for the nucleon gravitational form factors at $m_\pi = 170$ MeV, available for space-like momentum transfer squared up to 2 GeV, are explained in a natural way within the meson dominance approach. We carry out the proper Raman spin decomposition of the energy-momentum tensor and in each spin channel use a minimum number of resonances consistent with the perturbative QCD short-distance constraints. These constraints are related to the super-convergence sum rules, following from the asymptotic perturbative QCD fall-off of the form factors. The value of the nucleon D -term following from the fits is $-3.0(4)$. Next, we obtain the two-dimensional transverse gravitational densities of the nucleon in the transverse coordinate b . With the super-convergence sum rules, we derive new sum rules for these densities at the origin and for their derivatives, involving logarithmic weighting in the corresponding spectral density integrals. From analysis of the threshold behavior in the time-like region and the properties of the $\pi\pi \rightarrow N\bar{N}$ reaction, we infer the behavior of the transverse densities at asymptotically large coordinates. We also carry out the meson dominance analysis of the two- and three-dimensional mechanical properties of the nucleon (the pressure and stress) and explore their connection to the spectral densities via dispersion relations.

I. INTRODUCTION

The internal structure of the nucleon has been known to exist since the 1950's, when by means of the electron scattering it was found that it has a finite extension, non-trivial magnetic moments, or charge and currents distributions [1], which in a relativistically invariant formulation can be associated with matrix elements of electromagnetic currents [2]. A remarkable analysis of Frazer and Fulco [3–5] allowed to establish a connection between the electromagnetic nucleon structure and the $1^{--} \rho$ resonance in the charge form factors of both the pion and the nucleon, leading to the notion of the vector meson dominance [6] and the subsequent current-field identities [7, 8]. In the Breit frame, these matrix elements are identified as spatial charge and current distributions [9, 10], providing a physically intuitive picture of a nucleon resembling a droplet made of charged particles. This image has been ameliorated by introducing the transverse distributions, which correspond to viewing the nucleon in the perpendicular direction of a hadron boosted to the infinite momentum frame [11–16]. Then, remarkably, the transverse density of quarks of a particular flavor is manifestly positive definite [13, 14, 17], allowing for a probabilistic interpretation.

The considerations of the hadronic matrix elements of the stress-energy-momentum (SEM) tensor follow a similar path as the better known EM case, naturally extend-

ing to study the energy, momentum, and mass distributions in terms of the corresponding hadronic form factors. Matrix elements of SEM were first described by Kobzarev and Okun [18]. The idea of tensor meson dominance was introduced and applied by Freund [19] and by Sharp and Wagner [20], when describing the tensor meson exchange in the NN interaction. The analytic properties were described by Pagels [21], who suggested saturation by the 2^{++} mesons in the dispersion relations (see also [22]). Current-field identities were proposed in [23–26], and a connection to gravity [27, 28] was also given. An early mass radius estimate of the nucleon [29], based on the sidewise dispersion relations, yielded 0.7 fm.

While many of the relevant issues were essentially understood in the pre-QCD era, they remained dormant due to a lack of an experimental or lattice motivation. The situation has changed since Xiang-Dong Ji established the possibility of relating the deeply virtual Compton scattering (DVCS) to both EM current and SEM tensor via the moments of the corresponding Generalized Parton Distributions (GPDs) [30]. Later on, Polyakov and Weiss discovered the D -term [31], and Polyakov suggested to extend the nucleon picture by invoking its mechanical properties such as the mass, pressure or shear forces distributions, in an analogy to the classical elasticity theory [32], analyzed also in [33–37]. The mass and spin decomposition in terms of quarks and gluons has been addressed often, see [38–41], with the proviso that the separation depends on the renormalization scale and hence is scheme dependent. Asymmetric SEM in the polarized nucleon was considered in [42].

The depiction of the nucleon as a stable droplet in

* Wojciech.Broniowski@ifj.edu.pl

† earriola@ugr.es

mechanical equilibrium, as well as the relation of the D -term to moments of the pressure and the shear forces, constituting a genuine dynamical hadronic property, have triggered a lot of activity over the last years, extending the venerable EM current program and methods onto the SEM sector (see, e.g., [43] and references therein for a review and [44] for a transparent up-to-date perspective).

Numerous schemes and models have been proposed to describe the gravitational form factors (GFFs). Leading chiral corrections were addressed in the heavy baryon [45–48] or covariant baryon [49, 50] approaches. The large- N_c scaling was established in [51]. Estimates were made in the chiral quark soliton model [52], the Skyrme model [53], the MIT bag model [54], the holographic model [55], and in AdS/QCD [56, 57]. The QCD sum rules have also been applied [58, 59]. Valence quarks in the light front formulation were considered in [60], and a full QCD light front viewpoint was presented in [61]. Importantly, within perturbative QCD (pQCD), Tong, Ma, and Yuan [62, 63] have determined the leading asymptotic behavior of GFFs. A flavor decomposition using light-cone sum rules was presented in [64]. Holographic QCD was explored in [65, 66]. Quark and gluon decomposition of the nucleon GFFs was done in [67], and a Skyrme calculation was presented in [68].

On the experimental and phenomenological side, some constraints have been obtained via DVCS from CLAS at TJLab [69, 70], as well as from the GlueX [71] data for the J/ψ photoproduction [72]. Along these lines, an estimate of the proton mass radius [73–75] was obtained. In [76], a determination of GFFs from the Compton form factors was made. Holographic QCD modeling was carried out in [77]. A systematic Bayesian extraction of the proton mass radius based on photoproduction of vector charmoniums was made in [78].

The recent renewed interest in the gravitational structure of hadrons is spurred with the state-of-the-art lattice QCD calculations involving all the parton species [79–83] and at a low values of the pion mass, $m_\pi = 170$ MeV, close to the physical point. Similar studies for the gluon contribution to the trace anomaly form factor were carried out in [84] at higher values of m_π . These studies vastly improve on the previous lattice analyses of the quark GFFs of the nucleon [85–90].

In this paper we analyze the GFFs of the nucleon within a purely hadronic scheme, incorporating the quark-hadron duality principle via the meson¹ dominance, supplemented by short distance constraints from pQCD. These constraints imply super-convergence sum rules for the spectral densities associated with GFFs. The framework provides a large- N_c motivated functional expressions in the form of sums over meson pole masses,

taken from the Particle Data Group tables, and the residues fitted to the data. This large- N_c scheme, constrained with pQCD, has been successfully used in previous works for a variety of EM, SEM, and axial form factors, both for the pion and the nucleon [92]. Here we extend the method to describe the MIT lattice QCD data [79], using the insights of our previous analysis for the pion [93–95]. We use the data for the full form factors, involving the quark and gluon contributions. That way, one is not sensitive to the renormalization scale and scheme, as one deals with features of conserved currents.

We discuss in detail the two- and three-dimensional spatial distributions and the mechanical properties of the nucleon coming from our approach. We also relate them to the spectral densities via dispersion relations and obtain novel sum rules for the values of the above distributions and their derivatives at the origin. From the threshold behavior in the time-like region and the analyticity and unitarity properties of the $\pi\pi \rightarrow N\bar{N}$ amplitudes, we find the forms of the spatial distributions at asymptotically large coordinates.

When this work was in an advanced stage, a paper by Cao, Guo, Li, Yao [96] appeared, presenting a sophisticated Roy-Steiner equations analysis incorporating coupled channel unitarity, analyticity, and crossing for all channels, including $\pi\pi$, $K\bar{K}$ and $N\bar{N}$. The lack of experimental information for time-like momenta above the $N\bar{N}$ threshold requires to incorporate contributions from meson dominance to describe the data of [79].

II. GRAVITATIONAL FORM FACTORS OF THE NUCLEON

A. Stress-energy-momentum operator

We assume the definition of SEM following from the coupling to gravity, which provides a symmetric tensor from the outset. In the case of QCD, it coincides with the Belinfante-Rosenfeld symmetrized SEM [97, 98] (see also Appendix E of [99]), reading

$$\Theta^{\mu\nu} = \frac{i}{4} \bar{\Psi} \left[\gamma^\mu \overleftrightarrow{D}^\nu + \gamma^\nu \overleftrightarrow{D}^\mu \right] \Psi - F^{\mu\lambda a} F_{\lambda a}^\nu + \frac{1}{4} g^{\mu\nu} F^{\sigma\lambda a} F_{\sigma\lambda a} + \Theta_{\text{GF-EOM}}^{\mu\nu}, \quad (1)$$

where in the quantized case one has in addition the gauge-fixing and the equations-of-motion terms. Under a Lorentz transformation $x^\mu \rightarrow \Lambda_\alpha^\mu x^\alpha$, it transforms covariantly, $\Theta^{\mu\nu}(x) \rightarrow \Lambda_\alpha^\mu \Lambda_\beta^\nu \Theta^{\alpha\beta}(\Lambda^{-1}x)$, but not irreducibly. A naive decomposition into a traceless and traceful pieces

$$\Theta^{\mu\nu} = \Theta_{S,n}^{\mu\nu} + \Theta_{T,n}^{\mu\nu} \equiv \frac{1}{4} g^{\mu\nu} \Theta + \left[\Theta^{\mu\nu} - \frac{1}{4} g^{\mu\nu} \Theta \right], \quad (2)$$

with $\Theta = \Theta_\mu^\mu$, does not comply to a separate conservation of the two components, since $\partial_\mu \Theta_{S,n}^{\mu\nu} = -\partial_\mu \Theta_{T,n}^{\mu\nu} \neq 0$. In particular, this becomes a problem in the application of

¹ In this paper we use the definition of a meson in a broader sense, denoting a baryon number zero bound state or resonance, incorporating the quark model $q\bar{q}$ states, as well as glueballs or hybrids (see, e.g., Sec. 8.1.1 of [91]).

the meson dominance. A consistent decomposition where the two tensor components are conserved separately was proposed long ago by Raman [100], $\Theta^{\mu\nu} = \Theta_S^{\mu\nu} + \Theta_T^{\mu\nu}$, with

$$\Theta_S^{\mu\nu} = \frac{1}{3} \left[g^{\mu\nu} - \frac{\partial^\mu \partial^\nu}{\partial^2} \right] \Theta \implies \partial_\mu \Theta_S^{\mu\nu} = \partial_\mu \Theta_T^{\mu\nu} = 0. \quad (3)$$

The two irreducible tensors have a well-defined angular momentum, $J^{PC} = 0^{++}$ and 2^{++} , correspondingly. Although this decomposition involves an apparent non-locality, it does not lead to issues in our approach.

B. Matrix elements

With the symmetric SEM operator, the three gravitational form factors of the nucleon are defined through the matrix element in on-shell nucleons,

$$\begin{aligned} \langle p', s' | \Theta_{\mu\nu}(0) | p, s \rangle &= \bar{u}(p', s') \left[A(t) \gamma_{\{\mu} P_{\nu\}} \right. \\ &+ B(t) \frac{i P_{\{\mu} \sigma_{\nu\}} \rho q^\rho}{2m_N} + D(t) \frac{q_\mu q_\nu - g_{\mu\nu} q^2}{4m_N} \left. \right] u(p, s), \end{aligned} \quad (4)$$

where m_N is the nucleon mass, the Dirac spinors are normalized as $\bar{u}(p, s) u(p, s) = 2m_N$, $P = (p' + p)/2$, $q = p' - p$, $t = q^2$, $\sigma_{\mu\nu} = \frac{i}{2} [\gamma_\mu, \gamma_\nu]$, and $a_{\{\mu} b_{\nu\}} = \frac{1}{2} (a_\mu b_\nu + a_\nu b_\mu)$. Clearly, $P \cdot q = 0$ and $P^2 = m_N^2 - t/4$. The $A(t)$ form factor is chirally even whereas the $B(t)$ and $D(t)$ are chirally odd.

Through the use of the Gordon identity

$$2m \bar{u}' \gamma^\alpha u = \bar{u}' (2P^\alpha + i \sigma^{\alpha\rho} q_\rho) u, \quad (5)$$

the definition (4) can be equivalently written in different ways, which due to the mass term may mix the chiral properties. For instance,

$$\begin{aligned} \langle p', s' | \Theta_{\mu\nu}(0) | p, s \rangle &= \frac{1}{m_N} \bar{u}' \left[A(t) P_\mu P_\nu \right. \\ &+ J(t) i P_{\{\mu} \sigma_{\nu\}} \rho q^\rho + D(t) \frac{q_\mu q_\nu - g_{\mu\nu} q^2}{4} \left. \right] u. \end{aligned} \quad (6)$$

The form factors A , B , and J are related,

$$J(t) = \frac{A(t) + B(t)}{2}. \quad (7)$$

Another form of SEM that can be written is

$$\begin{aligned} \langle p', s' | \Theta_{\mu\nu}(0) | p, s \rangle &= \bar{u}' \left[2J(t) \gamma_{\{\mu} P_{\nu\}} \right. \\ &- B(t) P_\mu P_\nu \frac{1}{2m_N} + D(t) \frac{q_\mu q_\nu - g_{\mu\nu} q^2}{4m_N} \left. \right]. \end{aligned} \quad (8)$$

Normalizations are $A(0) = 1$ and $J(0) = \frac{1}{2}$ (this last condition is referred to as Ji's sum rule [30]). These

imply $B(0) = 0$, which is known as the vanishing of the ‘‘anomalous gravitomagnetic moment’’ of the nucleon [18]. Finally, the value $D(0)$ is the D -term [31], which is a dynamical quantity to be extracted from *ab initio* calculations or data (similarly to the magnetic moments or the axial coupling constant).

The trace of SEM, corresponding to the divergence of the dilation current, $J_\mu^D = \Theta_{\mu\nu} x^\nu$, and the trace anomaly of QCD, $\Theta_\mu^\mu = \partial^\mu J_\mu^D$, are related to the scalar gravitational form factor $\Theta(t)$,

$$\begin{aligned} \langle p', s' | T_\mu^\mu(0) | p, s \rangle &= \bar{u}(p', s') \Theta(t) \bar{u}(p, s), \\ \Theta(t) &= \frac{1}{m_N} \left[(m_N^2 - \frac{t}{4}) A(t) - \frac{3}{4} t D(t) + \frac{1}{2} t J(t) \right] \end{aligned} \quad (9)$$

with the condition $\Theta(0) = m_N$. From there one has

$$D(0) = \frac{4m_N}{3} [A'(0) - m_N \Theta'(0)]. \quad (10)$$

We extend the Raman decomposition introduced in Subsection II A to the nucleon case by explicitly choosing a mutually orthogonal basis in the tensor components. For the matrix element $\Theta^{\mu\nu} \equiv \langle p', s' | T^{\mu\nu}(0) | p, s \rangle$ it takes the form

$$\begin{aligned} \Theta^{\mu\nu} &= \Theta_S^{\mu\nu} + \Theta_T^{\mu\nu}, \\ \Theta_S^{\mu\nu} &= \frac{1}{3} Q^{\mu\nu} \bar{u}' \Theta(t) u, \\ \Theta_T^{\mu\nu} &= \Theta^{\mu\nu} - \frac{1}{3} Q^{\mu\nu} \bar{u}' \Theta(t) u, \end{aligned} \quad (11)$$

where the transverse tensor is defined as

$$Q^{\mu\nu} \equiv g^{\mu\nu} - q^\mu q^\nu / q^2 \quad (12)$$

and fulfills $Q_\mu^\mu = 3$ and $q^\mu Q_{\mu\nu} = 0$. Explicitly,

$$\begin{aligned} \Theta_T^{\mu\nu} &= \frac{\bar{u}' u}{m_N} \left[P^\mu P^\nu - \frac{P^2}{3} Q^{\mu\nu} \right] A(t), \\ &+ \frac{1}{m_N} \bar{u}' \left[i P^{\{\mu} \sigma^{\nu\}} \rho q_\rho - \frac{t}{6} Q^{\mu\nu} \right] u J(t), \end{aligned} \quad (13)$$

Thus, as already stressed, the Raman decomposition implements a separate conservation of the scalar and tensor parts, namely $q_\mu \Theta_S^{\mu\nu} = q_\mu \Theta_T^{\mu\nu} = 0$. We note that the apparent non-locality in Eq. (12) does not plague the considered quantities, as we only use the properties $q_\mu Q^{\mu\nu} = 0$ and $Q_\mu^\mu = 3$. The separate pole terms in $1/q^2$ cancel in the total sum by the condition $\Theta(0) = m_N A(0)$. Moreover, the A and J terms of Eq. (13) are separately traceless and conserved. Equation (13) can be cast in a form involving mutually orthogonal tensors, namely

$$\begin{aligned} \Theta_T^{\mu\nu} &= \frac{\bar{u}' u}{m_N} \left[P^\mu P^\nu - \frac{P^2}{3} Q^{\mu\nu} \right] \left(A(t) + \frac{t}{2P^2} J(t) \right) \\ &+ \frac{1}{m_N} \bar{u}' \left[i P^{\{\mu} \sigma^{\nu\}} \rho q_\rho - \frac{t}{2P^2} P^\mu P^\nu \right] u J(t). \end{aligned} \quad (14)$$

which has interesting unitarity properties in the time-like region (see Sect. II E).

From what has been said, Θ is the form factor of the scalar 0^{++} (trace anomaly) channel, while A and J correspond to the tensor channel 2^{++} . On the other hand, D mixes the spin quantum numbers and in that sense is less fundamental. From Eq. (9)

$$D(t) = \frac{1}{3} \left[\frac{4P^2}{t} A(t) + 2J(t) - \frac{4m_N}{t} \Theta(t) \right]. \quad (15)$$

The decomposition described above is needed for the meson saturation model, as it determines which mesons should be used for a particular form factor. We will therefore use Θ , A , and J as the basic form factors and obtain D from Eq. (15). Alternatively, one can use

$$-tD(t) = \frac{1}{3} \left[4m_N^2 \left(\frac{\Theta(t)}{m_N} - A(t) \right) - tB(t) \right], \quad (16)$$

which is the quantity appearing in the analysis of the mechanical properties.

C. Asymptotics from pQCD

Within pQCD, Tong, Ma, and Yuan [62, 63] derived the asymptotic formulas for the GFFs on the nucleon at large $-t$, which are

$$\begin{aligned} A(t) &\sim + \frac{\alpha(t)^2}{(-t)^2}, & J(t) &\sim + \frac{\alpha(t)^2}{(-t)^2} \\ B(t) &\sim - \frac{\alpha(t)^2}{(-t)^3}, & D(t) &\sim - \frac{\alpha(t)^2}{(-t)^3}. \end{aligned} \quad (17)$$

Here $\alpha(t)$ is the running strong coupling constant, which at the leading order reads

$$\alpha(t) = \frac{4\pi}{\beta_0 \ln(-t/\Lambda_{\text{QCD}}^2)}, \quad (18)$$

with $\beta_0 = (11N_c - 2N_f)/3 = 9$ for three active flavors. In Eq. (17), \pm indicates the overall sign (we do not attempt to give the values of the constants, which depend on the specific nucleon partonic distribution amplitudes (DAs)). As expected, the chirally odd form factors $B(t)$ and $D(t)$ fall off with an extra power of t as compared to the chirally even ones, $A(t)$ and $J(t)$. Actually, it has been found that the non-trivial relation $B(t) = 3D(t)$ holds asymptotically to leading order in pQCD [62, 63].

For the scalar (trace anomaly) form factor $\Theta(t)$, the situation is somewhat more complicated. From Eq. (9) $m_N \Theta(t) = m_N^2 A(t) + \frac{t}{4} (B(t) - 3D(t)) = \mathcal{O}(m_N^2 \alpha(t)^2 / t^2)$. However, the pQCD hard kernel behaves as $\alpha(t)^3 / (-t)^2$, and the presence of the soft end-point singularities in the nucleon DAs alters this behavior. In particular, Eq. (119) in [63], applying the DAs from [101], reads

$$\Theta(t) \sim - \frac{\alpha(t)^3}{(-t)^{3/2}} \log^2 \left(\frac{-t}{\Lambda_c^2} \right), \quad (19)$$

where $\Lambda_c \simeq 200$ MeV is a scale associated with DAs. Note a negative sign asymptotically. As concluded in [63], since $\Theta(0) = m_N > 0$, Eq. (19) requires a change of sign in $\Theta(-t)$ in the space-like domain $-t > 0$. Equations (17) are consistent, up to a weak logarithmic dependence, with the generic QCD counting rules [102, 103].

D. Dispersion relations and sum rules

Quite generally, the nucleon form factors $F(t)$ satisfy analytic properties: They are real in the space-like region, $t = -Q^2 \leq 0$, and possess a branch cut discontinuity starting at $s \geq 4m_\pi^2$, corresponding to the $\pi\pi \rightarrow N\bar{N}$ process below the $N\bar{N}$ threshold $s = 4m_N^2$. Hence, up to possible subtractions, a form factor $F(-Q^2)$ satisfies the dispersion relation

$$F(-Q^2) = \frac{1}{\pi} \int_{4m_\pi^2}^{\infty} ds \frac{\text{Im}F(s)}{s + Q^2}, \quad (20)$$

where $Q^2 = -t$ is the space-like momentum transfer squared.

The integrals in Eq. (20) converge if asymptotically $\text{Im}F(s)$ tends to zero sufficiently fast, which is the case in QCD. With the conditions (17), one finds immediately (by expanding $1/(s + Q^2) = 1/Q^2 - s/Q^4 + \dots$) the so-called super-convergence sum rules [93, 104–106],

$$\lim_{Q^2 \rightarrow \infty} Q^{2n} F(Q^2) = 0 \quad \Rightarrow \quad \int_{4m_\pi^2}^{\infty} ds s^{n-1} \text{Im}F(s) = 0, \quad n = 1, 2, \dots \quad (21)$$

This set of sum rules must be satisfied by the spectral density $\text{Im}F(s)/\pi$ of a given form factor. In particular, from (17) it follows that from pQCD A and J satisfy the sum rules with $n = 1, 2$, while B and D with $n = 1, 2, 3$. The presence of α , carrying additional damping, is needed for the highest n value. Indeed, the time-like large- s behavior corresponding to (17) is

$$\begin{aligned} \text{Im}A(s) &\sim + \frac{1}{s^2 L^3}, & \text{Im}J(s) &\sim + \frac{1}{s^2 L^3}, \\ \text{Im}B(s) &\sim - \frac{1}{s^3 L^3}, & \text{Im}D(s) &\sim - \frac{1}{s^3 L^3}, \end{aligned} \quad (22)$$

with the meaning $\text{Im}A(s) \equiv \text{Im}A(s + i\epsilon)$. In the derivation above, we have used the analytic continuation into the complex $t = s$ plane, $-t = \exp(-i\theta)|t|$, whence $\alpha(s + i\epsilon) = 4\pi/(\beta_0(L - i\pi))$, with the short-hand notation $L = \ln(s/\Lambda^2)$.

For the case of Θ ,

$$\text{Im}\Theta(s) \sim - \frac{1}{s^{3/2}} \frac{L_c^2}{L^3}, \quad (23)$$

where $L_c = \log(s/\Lambda_c^2)$. Therefore $\text{Im}\Theta(s)$ satisfies the sum rule (21) with $n = 1$ only.

Since all the considered GFFs of the nucleon satisfy (21) with $n = 1$, namely $\int_{4m_\pi^2}^{\infty} ds \text{Im}F(s) = 0$, all

the functions $\text{Im}F(s)$ cannot have a definite sign in the time-like domain $4m_\pi^2 \leq s < \infty$. This feature is analogous to the case of the gravitational spectral densities of the pion [93].

The charge-type sum rules have the form

$$F(0) = \frac{1}{\pi} \int_{4m_\pi^2}^{\infty} ds \frac{\text{Im}F(s)}{s}, \quad (24)$$

whereas the derivatives with respect to t at the origin are given by

$$\left. \frac{d^n F(t)}{dt^n} \right|_{t=0} = \frac{n!}{\pi} \int_{4m_\pi^2}^{\infty} ds \frac{\text{Im}F(s)}{s^n}, \quad (25)$$

from where, as is well known, it follows that precise modeling at low t requires a detailed knowledge of the spectral densities near the 2π production threshold.

E. Spectral densities at threshold

For our later analysis it is pertinent to determine some qualitative features of the spectral densities. In what follows, we will show that in the region $4m_\pi^2 \leq t \leq 4m_K^2$ (between the 2π and $K\bar{K}$ thresholds) the signs of the spectral functions corresponding to the Raman form factors Θ , J , $A + tJ/2P^2 = A + tB/4m_N^2$ and B are well defined and in fact positive. This is consistent with positivity in the space-like region at small $t = -Q^2$.

As already mentioned, the spectral functions corresponding to the nucleon GFFs start at $t = 4m_\pi^2$. They reflect the leading singularity in the $\pi\pi \rightarrow N\bar{N}$ process, which is not observable *below* the $N\bar{N}$ threshold $t = 4m_N^2$, but can be related to the observable pion form factors via unitarity and analyticity. The unitarity relations for the GFF were derived in [96] and can be written in several useful equivalent forms, for instance

$$\begin{aligned} \text{Im} \Theta(t) &= \frac{3\sigma_\pi f_{0,+}(t) \Theta_\pi^*(t)}{2(4m_N^2 - t)}, \\ \text{Im} J(t) &= \frac{3t^2 \sigma_\pi^5}{64\sqrt{6}} f_{2,-}(t) A_\pi^*(t), \\ \text{Im} A(t) + \frac{2t \text{Im} J(t)}{4m_N^2 - t} &= \frac{3t^2 \sigma_\pi^5}{32\sqrt{6}} f_{2,+}(t) A_\pi^*(t), \end{aligned} \quad (26)$$

where $\sigma_\pi = \sqrt{1 - 4m_\pi^2/t}$. Note that the combinations corresponding to the mutually orthogonal Raman-like decomposition of Eq. (14), involving the form factors $J(t)$ and $A(t) + tJ(t)/2P^2 = A(t) + tB(t)/4m_N^2$, comply naturally with the spin-flip and spin-non-flip $N\bar{N}$ amplitudes. From the above relations we immediately get

$$\begin{aligned} \text{Im} B(t) &= \frac{3t^2 m_N \sigma_\pi^5}{16(4m_N^2 - t)} \\ &\times \left[\frac{m_N \sqrt{2} f_{2,-}(t)}{\sqrt{3}} - f_{2,+}(t) \right] A_\pi^*(t). \end{aligned} \quad (27)$$

From Watson's theorem for the pion GFFs one has

$$\begin{aligned} \Theta_\pi(t) &= |\Theta_\pi(t)| e^{i\delta_{00}(t)}, \\ A_\pi(t) &= |A_\pi(t)| e^{i\delta_{02}(t)}, \end{aligned} \quad (28)$$

where δ_{00} and δ_{02} are the isoscalar S- and D-wave elastic scattering phase-shifts for the $\pi\pi \rightarrow \pi\pi$ process, respectively. While the elastic scattering takes place strictly below the $\pi\pi$ production threshold, i.e., for the process $2\pi \rightarrow 4\pi$ starting at $s = 16m_\pi^2$, it has been found over the years that in practice the inelasticity takes off at the $K\bar{K}$ threshold $s = 4m_K^2$.

Clearly, since $\text{Im} \Theta(t)$ is a real quantity, $f_{0,+}(t) = \pm |f_{0,+}(t)| e^{i\delta_{00}(t)}$, where the sign can be fixed by analyzing the $\pi N \rightarrow \pi N$ data in the physical region $s \geq (m_\pi + m_N)^2$ and analytically continuing to the unphysical region using unitarity and crossing. The net result is a rapid change of $|f_{0,+}(s)|$ around and above the threshold region, due to a subthreshold singularity at $s = 4m_\pi^2 - m_\pi^4/m_N^2$ stemming from the nucleon pole exchange contribution.

In the case of the D-wave form factors A and J , the result involves both the spin flip and non-flip $N\bar{N}$ scattering amplitudes. Similarly to the S-wave case, up to a sign they have a phase identical to the isoscalar D-wave $\pi\pi$ scattering phase-shift, $\delta_{20}(t)$, such that $f_{2,\pm}(s) = \pm |f_{2,\pm}(s)| e^{i\delta_{20}(s)}$. The values around the threshold have been determined in the venerable Karlsruhe-Helsinki (KH80) analysis [107] (numerical values are tabulated in [108]) and reviewed with uncertainties by the Bonn group [109]. The data analysis supports the plus sign in all channels, such that in the interval $4m_\pi^2 \leq t \leq 4M_K^2$ one has

$$\begin{aligned} \text{Im} \Theta(t) &= \frac{3\sigma_\pi |f_{0,+}(t)| |\Theta_\pi(t)|}{2(4m_N^2 - t)} > 0, \\ \text{Im} J(t) &= \frac{3t^2 \sigma_\pi^5}{64\sqrt{6}} |f_{2,-}(t)| |A_\pi(t)| > 0, \\ \text{Im} A(t) + \frac{2t \text{Im} J(t)}{4m_N^2 - t} &= \frac{3t^2 \sigma_\pi^5}{32\sqrt{6}} |f_{2,+}(t)| |A_\pi(t)| > 0, \\ \text{Im} B(t) &= \frac{3t^2 m_N \sigma_\pi^5 |A_\pi(t)|}{16(4m_N^2 - t)} \\ &\times \left[m_N \sqrt{\frac{2}{3}} |f_{2,-}(t)| - |f_{2,+}(t)| \right] > 0, \end{aligned} \quad (29)$$

where the last inequality follows from the data analysis and the Roy-Steiner solutions, yielding numerically $m_N \sqrt{2} |f_{2,-}(t)| / \sqrt{3} - |f_{2,+}(t)| > 0$. Finally, close to the threshold one has

$$\begin{aligned} \text{Im} \Theta(t) &\sim +(t - 4m_\pi^2)^{\frac{1}{2}}, \\ \text{Im} A(t), \text{Im} J(t), \text{Im} B(t) &\sim +(t - 4m_\pi^2)^{\frac{5}{2}}, \end{aligned} \quad (30)$$

where the corresponding proportionality constants are *positive* and, besides the $\pi\pi \rightarrow N\bar{N}$ amplitudes, also involve the pion form factors at the threshold $s = 4m_\pi^2$.

Whereas their normalization is $A_\pi(0) = 1$ and $\Theta_\pi(0) = 2m_\pi^2$, from the meson dominance formulas of our previous work [94] one gets

$$\begin{aligned} A_\pi(4m_\pi^2) &= \frac{m_{f_2}^2}{m_{f_2}^2 - 4m_\pi^2} \sim 1 + \frac{4m_\pi^2}{m_{f_2}^2}, \\ \Theta_\pi(4m_\pi^2) &= 2m_\pi^2 + \frac{4m_\pi^2 m_\sigma^2}{m_\sigma^2 - 4m_\pi^2} \sim 6m_\pi^2. \end{aligned} \quad (31)$$

F. Problem of the high-energy completion

Quite generally, one might hope that the use of the dispersion relations where $\text{Im}F(s)$ is known up to a sufficiently large value of s , such as the $N\bar{N}$ threshold $s_N = 4m_N^2$, allows one to determine accurately the form factor in the space-like region. Taking for definiteness D , one can write

$$D(-Q^2) = \frac{1}{\pi} \int_{4m_N^2}^{4m_N^2} ds \frac{\text{Im}D(s)}{s + Q^2} + \frac{1}{\pi} \int_{4m_N^2}^{\infty} ds \frac{\text{Im}D(s)}{s + Q^2}, \quad (32)$$

where the spectral integral has been divided into a ‘‘better known’’ part below s_N and a ‘‘less known’’ part above s_N . Unitarity provides the absorptive part $\text{Im}D(s)$ up to the $K\bar{K}$ threshold in terms of the $\pi\pi \rightarrow N\bar{N}$ amplitudes $f_{+,0}(s)$ and $f_{\pm,2}(s)$ and the pion form factors in the time-like region, $A_\pi(t)$ and $\Theta_\pi(t)$. However, the high- s part is not known accurately. Alternatively, one could use subtracted dispersion relations, but then the predictive power is diminished. For instance, $D(0)$ would be taken as a low-energy constant, but its value not predicted.

The recent work of [96] based on dispersion relations and incorporating a full Roy-Seiner analysis with all the pertinent channels, including pions, kaons, and nucleons, has indeed reported a slow convergence of the dispersive integrals when confronting with the lattice QCD data [79] for $Q^2 \leq 2\text{GeV}^2$. To overcome this contingency, additional narrow resonances have been included in the analysis of [96].

With this guidance, in the next section we retake the old idea of the meson dominance to describe the lattice data with a minimal but realistic amount of information.

III. MESON DOMINANCE APPROACH

Along the years, the idea of the resonance saturation has been extended to all possible quantum number channels. In our case, we are concerned with the scalar- and tensor meson dominance. We first sketch the basic features of the approach and then go into a detailed analysis, exploring the predictive power of the meson dominance approach for both GFFs and the mechanical properties of the nucleon.

A. Basic features of meson dominance

The meson dominance approach, motivated by the large- N_c arguments, is known to work remarkably well for hadronic form factors at intermediate space-like momenta (see, e.g., [92] and references therein).² A form factor F is approximated as, in general, an infinite sum over narrow resonances in the appropriate channel,

$$F(-t) = \sum_i \frac{c_i}{m_i^2 - t}. \quad (33)$$

Here m_i denotes the resonance mass and c_i its coupling. Alternatively, the spectral strength is given by

$$\frac{1}{\pi} \text{Im}F(-t) = \sum_i c_i \delta(m_i^2 - t). \quad (34)$$

The short distance (or large $-t$) constraints (also known as the counting rules) impose relations between c_i 's and m_i 's. In particular, if $\lim_{t \rightarrow -\infty} (-t)^n F(t) = 0$, one obtains the constraints

$$\sum_i c_i m_i^{2k} = 0, \quad k = 0, \dots, n-1, \quad (35)$$

which here are just a manifestation of the superconvergence sum rules (21).

B. Current-field identities

In the particular SEM case, the current-field identity [24–26] is the simplest way to express the scalar- and tensor meson dominance,

$$\Theta^{\mu\nu} = \sum_S \frac{1}{3} f_S (\partial^\mu \partial^\nu - g^{\mu\nu} \partial^2) S + \sum_T f_T m_T^2 T^{\mu\nu}, \quad (36)$$

where S and $T^{\mu\nu}$ are the scalar 0^{++} and tensor 2^{++} meson fields, respectively, with $T^{\mu\nu} = T^{\nu\mu}$ and $T_\mu^\mu = 0$. On-shell, the fields have masses m_S and m_T , respectively, and $\partial^\mu T_{\mu\nu} = 0$ (for the complete Lagrangian see, e.g., [110, 111]). Defining the corresponding sources as J_S and $J_T^{\mu\nu}$, one gets the equations of motion,

$$(\partial^2 + m_S^2)S = J_S, \quad (37)$$

$$(\partial^2 + m_T^2)T^{\mu\nu} = J_T^{\mu\nu} + \text{dist.}, \quad (38)$$

² On the contrary, the determination of the time-like behavior of the form factors usually requires abundant data in a wide interval and, from the dispersive point of view, an extrapolation to the unphysical region. Fortunately, the impact of the time-like details on the space-like region considered here is mild.

where the distributional contributions are deltas and derivatives located at $x = 0$. Passing to the momentum space, we get formally (up to polynomials in q)

$$\begin{aligned} \langle A|\Theta^{\mu\nu}|B\rangle &= \sum_S \frac{f_S}{3} \frac{g^{\mu\nu}q^2 - q^\mu q^\nu}{m_S^2 - q^2 - i\epsilon} \langle A|J_S|B\rangle \\ &+ \sum_T f_T \frac{m_T^2}{m_T^2 - q^2 - i\epsilon} \langle A|\sum_\lambda \epsilon_\lambda^{\mu\nu} \epsilon_{\alpha\beta}^\lambda J_T^{\alpha\beta}|B\rangle, \end{aligned} \quad (39)$$

where $\epsilon_\lambda^{\mu\nu}$ is the spin-2 polarization tensor, which is symmetric, $\epsilon_\lambda^{\mu\nu} = \epsilon_\lambda^{\nu\mu}$, traceless $g_{\mu\nu}\epsilon_\lambda^{\mu\nu} = 0$, and transverse $q_\mu\epsilon_\lambda^{\mu\nu} = 0$. Clearly, the separate conservation of the scalar and tensor contributions is manifest according to the Raman decomposition.

C. t-channel unitarity

From a field theory point of view, the meson dominance formula should not be taken literally, as it does not incorporate the notion of subtractions or the pQCD high-momentum behavior. Besides, it is well known that higher spin fields have certain problems, particularly due to the role played by the off-shell behavior of the propagators [110, 111]. The simplest way to avoid these issues is to use the meson dominance for the absorptive parts in the dispersion relations, where by construction the meson resonances are on the mass shell (see, e.g., [93] for the pion GFF case). Then, one can fix the minimal number of subtractions needed to satisfy the short distance constraints (counting rules) imposed by pQCD.

It is far more practical to compute the absorptive part of the form factor in the time-like region, where for the graviton we have $g \rightarrow R \rightarrow N\bar{N}$. At $q^2 \rightarrow s + i\epsilon$ we then have

$$\frac{1}{\pi} \text{Im} \langle N\bar{N}|\Theta^{\mu\nu}|0\rangle = \sum_R \langle N\bar{N}|R\rangle \langle R|\Theta^{\mu\nu}|0\rangle \delta(m_R^2 - s), \quad (40)$$

and later will reconstruct the dispersive part from the dispersion relation with suitable subtraction constants. The vacuum to hadron transition amplitudes are

$$\langle S|\Theta^{\mu\nu}|0\rangle = \frac{1}{3} f_S q^2 Q^{\mu\nu}, \quad \langle T|\Theta^{\mu\nu}|0\rangle = f_T m_T^2 \epsilon_\lambda^{\mu\nu}, \quad (41)$$

where the extra factor of $1/3$ in the scalar case is conventional, chosen such that $\langle S|\Theta|0\rangle = f_S q^2$. The *on-shell* couplings of the resonances to the $N\bar{N}$ continuum are conventionally taken as [112]

$$\begin{aligned} \langle S|N\bar{N}\rangle &= g_{SNN}, \\ \langle T|N\bar{N}\rangle &= \epsilon_\lambda^{\alpha\beta} \bar{v} \left[g_{TNN} P^{\{\alpha\gamma\beta\}} + f_{TNN} P^\alpha P^\beta \right] u. \end{aligned} \quad (42)$$

with v denoting the \bar{N} spinor. Thus, we get

$$\begin{aligned} \frac{1}{\pi} \text{Im} \langle N\bar{N}|\Theta^{\mu\nu}|0\rangle &= \sum_S \frac{g_{SNN} f_S}{3} \delta(m_S^2 - q^2) m_S^2 Q^{\mu\nu} \\ &+ \sum_{T,\lambda} \epsilon_\lambda^{\alpha\beta} P^{\{\alpha\gamma\beta\}} \epsilon_\lambda^{\mu\nu} g_{TNN} f_T m_T^2 \delta(m_T^2 - q^2) \\ &+ \sum_{T,\lambda} \epsilon_\lambda^{\alpha\beta} P_\alpha P_\beta \epsilon_\lambda^{\mu\nu} f_{TNN} f_T m_T^2 \delta(m_T^2 - q^2), \end{aligned} \quad (43)$$

which naturally complies with a separate conservation for each term, yielding zero when contracted with q^μ . The sum over the tensor polarizations is given by [113, 114]

$$\sum_\lambda \epsilon_\lambda^{\alpha\beta} \epsilon_\lambda^{\mu\nu} = \frac{1}{2} (Q^{\mu\alpha} Q^{\nu\beta} + Q^{\nu\alpha} Q^{\mu\beta}) - \frac{1}{3} Q^{\mu\nu} Q^{\alpha\beta}. \quad (44)$$

The on-shell condition $P \cdot q = 0$ implies $P_\alpha Q^{\alpha,\beta} = P^\beta$ and $\bar{u}' q u = 0$ yields $\gamma_\alpha Q^{\alpha,\beta} = \gamma^\beta$, hence we obtain

$$\begin{aligned} \sum_\lambda \epsilon_\lambda^{\alpha\beta} P_\alpha P_\beta \epsilon_\lambda^{\mu\nu} &= P^\mu P^\nu - \frac{1}{3} P^2 Q^{\mu\nu}, \\ \sum_\lambda \epsilon_\lambda^{\alpha\beta} P^{\{\alpha\gamma\beta\}} \epsilon_\lambda^{\mu\nu} &= P^{\{\mu\gamma\nu\}} - \frac{1}{3} Q^{\mu\nu} \not{P} \end{aligned} \quad (45)$$

(cf. the tensor structure in Eq. (8); the other combination is compatible with Gordon's identity, Eq. (5)). Therefore, in the narrow resonance, large- N_c motivated approach we get

$$\begin{aligned} \frac{1}{\pi} \text{Im} J(s) &= \frac{1}{2} \sum_T g_{TNN} f_T m_T^2 \delta(m_T^2 - q^2), \\ \frac{1}{\pi} \text{Im} B(s) &= -2m_N \sum_T f_{TNN} f_T m_T^2 \delta(m_T^2 - q^2), \\ \frac{1}{\pi} \text{Im} \Theta(s) &= \sum_S g_{SNN} f_S m_S^2 \delta(m_S^2 - q^2), \end{aligned} \quad (46)$$

and $\text{Im} A(s) = 2\text{Im} J(s) - \text{Im} B(s)$, where, as expected, the corresponding spectral strengths get contributions exclusively from the proper spin states: A and B from spin-2 and Θ from spin-0.

D. Minimal hadronic saturation

In practice, to avoid proliferation of parameters, one tries to limit the number of mesons (recall footnote 1) to the lowest possible number consistent with the constraints.³ Note, however, that more precise model-

³ For instance, with two mesons included and the $1/(-t)^2$ asymptotic behavior, the condition $c_1 + c_2 = 0$ cancels the $1/(-t)$ behavior, yielding $F(t) = F(0) m_1^2 m_2^2 / [(m_1^2 - t)(m_2^2 - t)]$. The construction based on Eqs. (33,35) provides a natural interpretation for the widely used multipole fits, for instance the dipole form for the nucleon electromagnetic form factors, since $1/(m^2 - t)^2$ is numerically close to $1/[(m_1^2 - t)(m_2^2 - t)]$ for a suitably chosen m in the considered range of $-t$.

ing in the time-like region typically utilizes more resonances and incorporates their width, in an effort to reproduce the spectra. An example is the Gounaris-Sakurai model [115, 116] for the pion charge form factor, where as many as four ρ resonances are used, including the width effects. However, in the space-like region considered here with the aim to understand the lattice QCD data, the meson dominance modeling is not sensitive to the details of the time-like region.

In this work we use the asymptotic forms of Eq. (17) as an inspiration to build the meson saturation model. We do not take into account the log corrections, as they would require more precise modeling of the spectral densities, not relevant for the low values of $0 < -t < 2$ GeV, and also would increase the number of free parameters. Ignoring the log corrections from $\alpha(t)$ weakens the asymptotic convergence and causes a lack of the sum rule (21) with the highest value of n in each channel.⁴ As stated above, in a minimum model, one uses the lowest possible number of resonances needed to implement the large $-t$ (the short-distance) constraints, as well as the behavior at $t = 0$. This number is determined by $B(t)$. Since $B(0) = 0$ and at $t \rightarrow -\infty$ we have $B(t) \sim 1/(-t)^3$, the lowest number of resonances is four, which leads to the form

$$B(t) = \frac{c_B t}{(1 - t/m_{f_2}^2)(1 - t/m_{f_2'}^2)(1 - t/m_{f_2''}^2)(1 - t/m_{f_2'''}^2)}, \quad (47)$$

where $f_2 \dots f_2'''$ are the four lowest mass 2^{++} mesons.

We assume, accordingly, that the A and J channels couple to the same four resonances, but with different couplings, such that $A(0) = 1$, $J(0) = \frac{1}{2}$, and asymptotically Eqs. (17) hold. Thus, we take⁵

$$\begin{aligned} A(t) &= \frac{1 - c_A t + c_2 t^2}{(1 - t/m_{f_2}^2)(1 - t/m_{f_2'}^2)(1 - t/m_{f_2''}^2)(1 - t/m_{f_2'''}^2)}, \\ J(t) &= \frac{1 - c_J t + c_2 t^2}{2(1 - t/m_{f_2}^2)(1 - t/m_{f_2'}^2)(1 - t/m_{f_2''}^2)(1 - t/m_{f_2'''}^2)}. \end{aligned} \quad (48)$$

Equations (7) and the above formulas are consistent with Eq. (47) with $c_B = c_J - c_A$.

In the scalar channel, where $\Theta(0) = m_N$, we take for simplicity two resonances,

$$\Theta(t) = \frac{m_N}{(1 - t/m_\sigma^2)(1 - t/m_{f_0}^2)}, \quad (49)$$

where the power agrees with the counting rules for the corresponding pQCD kernel. Here m_σ is an effective mass

of the sigma meson and f_0 is the scalar resonance $f_0(980)$. Again, more precise modeling would require more realistic and complicated spectral functions, which is expected to be irrelevant in the space-like momentum region explored in lattice QCD simulations.

Naturally, Eqs. (48,49) can be written, via pole expansion of a meromorphic function, as sums of simple poles of the form (33), where the residues “conspire” in such a way that the short-distance constraints are satisfied. Some properties of the fitted functions are presented in Appendix A.

E. Fitting procedure

We treat m_σ , c_A , c_J , and c_2 as free model parameters. The mass of f_0 is fixed at $m_{f_0} = 980$ MeV, while for the tensor masses we probe two sets, largely differing in the second and third excited states (all masses in GeV),

$$\begin{aligned} \text{I:} \quad & m_{f_2} = 1.275, m_{f_2'} = 1.517, m_{f_2''} = 1.936, m_{f_2'''} = 2.011, \\ \text{II:} \quad & m_{f_2} = 1.275, m_{f_2'} = 1.430, m_{f_2''} = 1.517, m_{f_2'''} = 1.565, \end{aligned} \quad (50)$$

with set I corresponding to the first four entries in the PDG (Particle Data Group) [117] summary tables, and set II to the PDG listings. Comparing the fits made with sets I and II allows for an estimate of a “systematic” error in our analysis. It turns out that in the range of the space-like lattice data, this error is much smaller (relatively, a few percent) from the statistical error originating from the uncertainty in the data. For this reason we combine the systematic and statistical errors in the results presented below.

Since the lattice data correspond to $m_\pi = 170$ MeV, we use correspondingly an increased nucleon mass, $m_N = 970$ MeV [118]. We do not change the values of the resonance masses, as they are expected to be at the level of a few percent. Accordingly, our results for the nucleon GFFs correspond to $m_\pi = 170$ MeV. Based on our experience for the pion [93], we anticipate that the results of the chiral evolution to the physical point $m_\pi = 140$ MeV are not very significant, at a level of a few percent for the values of the model parameters.

F. Results

The joint fit to the available MIT lattice data for A , J , and D (for which we use Eq. (15)) yields for set I

$$\begin{aligned} c_A &= 0.47(4) \text{ GeV}^{-2}, \quad c_J = 0.69(5) \text{ GeV}^{-2}, \\ c_2 &= 0.10(4) \text{ GeV}^{-4}, \quad m_\sigma = 0.64(4) \text{ GeV}, \end{aligned} \quad (51)$$

and for set II

$$\begin{aligned} c_A &= 0.83(6) \text{ GeV}^{-2}, \quad c_J = 1.12(7) \text{ GeV}^{-2}, \\ c_2 &= 0.25(5) \text{ GeV}^{-4}, \quad m_\sigma = 0.64(4) \text{ GeV}, \end{aligned} \quad (52)$$

⁴ For the electromagnetic case, models including the log corrections, thus satisfying all the super-convergence sum rules, were explored in [106].

⁵ For a similar construction of the ansatz for the case of the nucleon electromagnetic form factors see, e.g., [92].

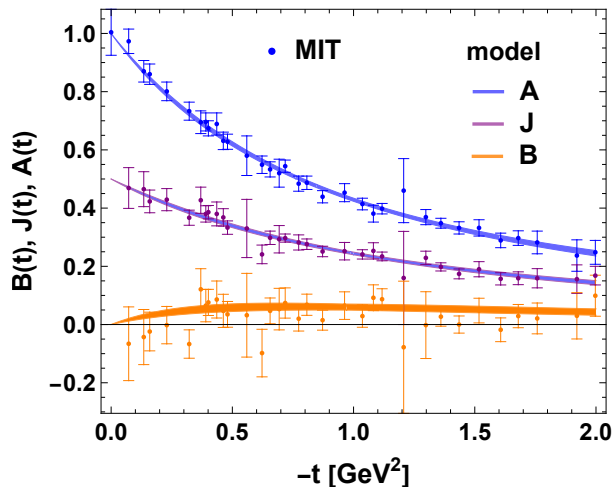


FIG. 1. Gravitational form factors of the nucleon, A , J , and B , plotted as functions of the space-like momentum transfer $-t$. The MIT lattice QCD data for A and J are taken from [79], while those for B follow from the relation $B = 2J - A$ with errors added in quadrature. The meson dominance model fit is shown with the error bands, whose widths reflect the uncertainty in the parameters (see the text for details). The MIT data and the fits are for $m_\pi = 170$ MeV.

where the errors are statistical. The change of the c_i coefficients between the two sets follows the features explained in Appendix A. For both sets the values of χ^2/DOF are ~ 0.4 , indicating that the nature of the lattice data errors involves systematic uncertainty and/or correlations. In our fits, the values of c_A , c_J , and c_2 change to compensate for the effect of different masses of the m_{f_2} states in parameterizations I and II in the range of the data. The value of m_σ is in agreement within the uncertainties with the fit for the pion case in [93], where we obtained $m_\sigma = 0.65(3)$ GeV at $m_\pi = 170$ MeV.

The correlation matrix, for the rows and columns in the sequence of parameters given above, is, for case I,

$$\rho = \begin{pmatrix} 1 & 0.7 & -0.9 & 0.3 \\ 0.7 & 1 & -0.8 & 0.1 \\ -0.9 & -0.8 & 1 & -0.2 \\ 0.3 & 0.1 & -0.2 & 1 \end{pmatrix} \quad (53)$$

(for case II it is similar). We note that m_σ is weakly correlated to the other parameters, as this correlation occurs only by their common appearance in D . On the other hand, the c_i coefficients are strongly correlated. The correlations are taken into account in the error propagation to the form factors, shown in the figures below with the bands, indicating the 68% confidence levels.

In Fig. 1 we plot the form factors A , J , and B . We get a proper description of the MIT lattice data [79]. The bands in the figures indicate the combined systematic error from the two choices of the tensor meson spectrum (50), and from the statistical error reflecting the uncertainties in the fitted lattice data. We note that the

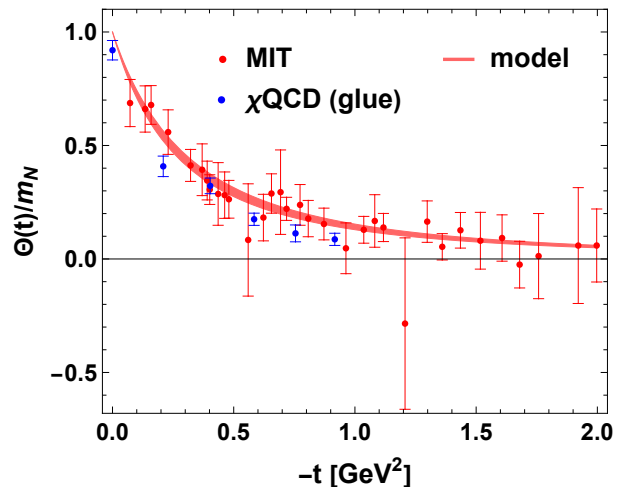


FIG. 2. Scalar (trace anomaly) gravitational form factor Θ of the nucleon, divided with the nucleon mass m_N and plotted as a function of the space-like momentum transfer $-t$. The red data points labeled MIT are obtained from the data [79] via the relation (9), with errors added in quadrature. The meson dominance model fit is shown with the error band, whose width reflects the uncertainty of the effective σ mass (see text for details). The MIT data and the fit are for $m_\pi = 170$ MeV. We also show (blue points), for a rough comparison, the glue contribution to the trace anomaly form factor at $m_\pi = 253$ MeV from the χ QCD Collaboration [84].

systematic error for A and J , estimated by comparing sets I and II, is significantly smaller from the statistical error (a few percent), reflecting the fact that at the available range of $-t$ one cannot resolve the details of the model.

For the case of B , the values for the data were obtained via the relation (7), with the errors added in quadrature. We note the smallness of B , yet it is significantly larger from zero at $-t > 0$ compared to the error bars. The LHPC collaboration [89] computed the quark parts of the GFF's and found a similar trend. Interestingly, the observed smallness was predicted long ago by Renner [119] within the quark model. The feature is reproduced in the Chiral Soliton model [120] and less accurately in the Skyrme model [53].

The scalar GFF $\Theta(t)$ is plotted in Fig. 2, where the data were obtained from [79] via the combination of Eq. (9) with errors added in quadrature. The minimum meson dominance formula (49) fits the data properly, and as already remarked, with m_σ compatible within uncertainty to the case of the pion GFFs [93]. The present lattice errors are too large and the range of $-t$ too small to test more precisely the asymptotic behavior of Eq. (19).

Figure 3 shows the form factor D . In this case the model description follows from Eq. (15). Again, we can see a proper description of the MIT lattice data, with the error band getting broader as $-t$ is decreased. For comparison, we also show the physical data from deeply virtual Compton scattering (DVCS) on the proton measured

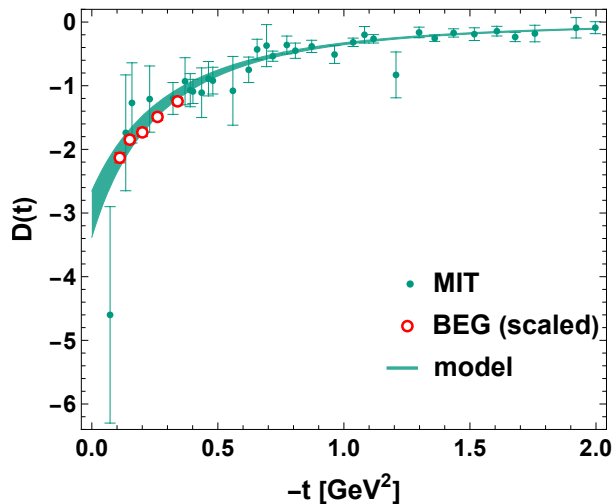


FIG. 3. Gravitational form factor D of the nucleon, plotted as a function of the space-like momentum transfer $-t$. The MIT lattice QCD data are from [79]. The meson dominance model fit is shown with an error band whose width reflects the uncertainty in the parameters (see the text for details). The MIT lattice data and the fit are for $m_\pi = 170$ MeV. The points labeled BEG (open circles) are from DVCS obtained for the quark part in [70] and rescaled as described in the text.

at CLAS [69] and extracted in [70] for the quark part of $D(t)$. The data points were obtained from Fig. 11 of [43] by utilizing the relation $D_{u+d} = \frac{18}{25}\mathcal{C}_H(t)$, cf. Eq. (40) in [43]. To compare to $D(t)$ including the gluons, we assume that the form factors for the quarks and gluons have the same shape in $-t$,⁶ which allows for the scaling $D(t) = (\langle x \rangle_q + \langle x \rangle_g) / \langle x \rangle_q D_q(x)$. We take the world average $\langle x \rangle_q \simeq 0.41$. Thus extracted DVCS data lie within the band corresponding to our fit to the MIT data.

Note that in our model, at space-like momenta, A , J , B , and Θ are positive-definite, whereas D is negative-definite. Hence all form factors have a definite sign. Except for Θ , which according to Eq. (19) should change the sign, the obtained sign behavior is compatible with the asymptotics of Eq. (17).

G. D -term

The obtained value of the D -term corresponding to the plot in Fig. 3 is

$$D(0) = -3.0(4). \quad (54)$$

⁶ This in general may not be the case, as the form factors $\bar{c}_a(t)$, dependent on the renormalization scheme and scale, may be different for various parton species. However, in models where all the gluons are radiatively generated by the QCD evolution from a low quark model scale, the shapes of the gluon and quark form factors are equal [121].

The mechanical radius, as defined in [122], is

$$\langle r^2 \rangle_{\text{mech}} = \frac{6D(0)}{\int_0^\infty d(-t)D(t)} = [0.72(5) \text{ fm}]^2, \quad (55)$$

which is a value comparable to other estimates (see [123] for a recent review).

IV. TRANSVERSE DENSITIES

A. Motivation

While not directly accessible in experiment, the transverse two-dimensional densities of hadrons, evaluated in the infinite momentum frame, were promoted in [11–16] as the proper spatial distributions, dependent only on the intrinsic features of the probed state. The main advantage is a possibility, in the case where positivity holds, of a probabilistic interpretation of the parton distributions. In particular, the transverse density of quarks of a particular flavor is manifestly positive definite [13, 14, 17]. Analogously, the transverse Θ^{++} distribution is also positive definite (in the light-cone gauge) for any hadronic state, as shown generally in [95],

$$\int dx^- \Theta^{++}(b, x^-)|_{x^+=0} > 0. \quad (56)$$

Moreover, the transverse densities are related to the transverse mechanical properties, as elaborated below, which is of attractive interpretational merits.

B. Definitions

We use the light-cone coordinate system in the convention $a^\pm = 1/\sqrt{2}(a^0 \pm a^3)$. The infinite-momentum Breit frame (IMBF), also known as the Drell-Yan frame [124], is defined as

$$\begin{aligned} P^1 = P^2 = 0, \quad P^- &= \frac{m_N^2 - \frac{1}{4}t}{2P^+}, \\ q^+ = q^- = 0, \end{aligned} \quad (57)$$

with $P^+ = p^+ = p'^+ \rightarrow \infty$. In this frame, the Dirac spinors are

$$u(p, s) = \sqrt{p^+} \begin{pmatrix} 1 \\ \sigma_3 \end{pmatrix} \chi_s, \quad (58)$$

with χ_s denoting a two-component Pauli spinor and $\bar{u}'(p', s')u(p, s) = 2P^+ \delta_{ss'}$. IMBF is used in the formulas of this and the following subsections.

The matrix elements in the transverse coordinate space are defined via the two-dimensional Fourier transforms of the basic SEM matrix elements, namely,

$$T^{\mu\nu}(b) = \int \frac{d^2 q_\perp}{(2\pi)^2 2P^+} e^{-i\mathbf{b} \cdot \mathbf{q}_\perp} \langle p', s | \Theta_{\mu\nu}(0) | p, s \rangle. \quad (59)$$

For the $++$ component one finds

$$T^{++}(b) = \frac{P^{+2}}{m_N} \int \frac{d^2 q_\perp}{(2\pi)^2} e^{-i\mathbf{b}\cdot\mathbf{q}_\perp} A(-q_\perp^2), \quad (60)$$

hence it depends only on the A form factor. We may thus define

$$A(b) = \int \frac{d^2 q_\perp}{(2\pi)^2} e^{-i\mathbf{b}\cdot\mathbf{q}_\perp} A(-q_\perp^2) = \int_0^\infty \frac{q_\perp dq_\perp}{2\pi} J_0(b q_\perp) A(-q_\perp^2), \quad (61)$$

with an obvious normalization $\int_0^\infty 2\pi b db A(b) = 1$. According to Eq. (60), $A(b)$ can be interpreted as the distribution of P^{+2}/m_N in the transverse coordinate plane.

For the trace anomaly form factor we obtain

$$\Theta(b) \equiv 2T^{+-}(b) - T^{11}(b) - T^{22}(b) = \int \frac{d^2 q_\perp}{(2\pi)^2} e^{-i\mathbf{b}\cdot\mathbf{q}_\perp} \Theta(-q_\perp^2), \quad (62)$$

with $\int_0^\infty 2\pi b db \Theta(b) = m_N$.

The transverse-coordinate spin density along the z -axis, $J(b)$, is evaluated as (cf. Eq. [76] of [125] and the discussion of the associated symmetric prescription for $\Theta^{\mu\nu}$)

$$J(b) = \int \frac{d^2 q_\perp}{(2\pi)^2} e^{-i\mathbf{q}_\perp\cdot\mathbf{b}} \left[J(-q_\perp^2) + q_\perp^2 \frac{dJ(-q_\perp^2)}{dq_\perp^2} \right] = \frac{b}{4\pi} \int_0^\infty dq_\perp J_1(b q_\perp) [q_\perp^2 J(-q_\perp^2)], \quad (63)$$

where in getting to the last line we have integrated by parts and used the relation for the Bessel functions, $\frac{d}{dz} J_0(z) = -J_1(z)$.

The transverse density of D is related to the transverse (mechanical) components of SEM, discussed in detail in Section V.

C. Dispersive sum rules and the $b \rightarrow 0$ limit

For the transverse density defined via

$$F(b) = \int \frac{d^2 q_\perp}{(2\pi)^2} e^{-i\mathbf{b}\cdot\mathbf{q}_\perp} F(-q_\perp^2) = \frac{1}{2\pi} \int q_\perp dq_\perp J_0(b q_\perp) F(-q_\perp^2), \quad (64)$$

the dispersion relation yields, after carrying out the q_\perp integration (which can be interchanged with the integration over s for convergent integrals), the following formula [126]:

$$F(b) = \frac{1}{2\pi^2} \int_{4m_\pi^2}^\infty ds K_0(b\sqrt{s}) \text{Im} F(s). \quad (65)$$

For the special case of the J form factor, with the definition (63), one finds instead

$$J(b) = \frac{b}{4\pi^2} \int_{4m_\pi^2}^\infty ds \sqrt{s} K_1(b\sqrt{s}) \text{Im} J(s). \quad (66)$$

Because at asymptotically large argument the Bessel functions $K_n(z) \sim e^{-z} \sqrt{\pi/(2z)}$, integrals in (65,66) are convergent.

At $b \rightarrow 0$, the integration kernel in (65) is singular, since $K_0(b\sqrt{s}) \sim -\frac{1}{2} \log(b^2 s) + \text{const} + \mathcal{O}(b^2 \log b)$. However, the $\log(b^2)$ term and the constant are canceled via the super-convergence sum rule (21) for $n = 1$. This yields the general, a model independent sum rule

$$F(b=0) = -\frac{1}{4\pi^2} \int_{4m_\pi^2}^\infty ds \log s \text{Im} F(s), \quad (67)$$

holding for $F = A, B, \Theta$, and D . Equation (67) may be viewed as a spectral sum rule, which due to the $-\log s$ weight⁷ collects contributions from the whole physical region in s , and not as one might naively expect, predominantly from the low- s values. At lower s , this weight is positive, and at large s it is negative, but since the spectral strength has no definite sign as implied by the super-convergence sum rule, it is not possible to make a priori statements concerning the sign of $F(b=0)$.

Moreover, there is an important methodological warning following from the Eq. (67) which we have not seen discussed in the literature. The formula indicates a strong sensitivity also to the high- s part of the spectrum, which at present is largely unknown and dependent on the particular model used. Another way to see this more directly is from Eq. (64) and noticing that the tails of the form factors in Figs. 1-3 sticking outside of the range of the data, and still much below the in principle known pQCD asymptotics, are strong. This uncertainly must be kept in mind when obtaining the transverse densities from models or fits to data, including the mechanical properties discussed in Sect. V.

For the curvature at $b = 0$, an analogous reasoning to the one leading to Eq. (67) can be carried out with the sum rule (21) for $n = 2$, which results in

$$F(b) = F(b=0) - \frac{b^2}{16\pi^2} \int_{4m_\pi^2}^\infty ds s \log s \text{Im} F(s) + \mathcal{O}(b^4 \log b). \quad (68)$$

According to the discussion in Subsection IIC, with proper pQCD constraints, it holds for $F = A, B$, and

⁷ One does not need to keep a dimensionful scale here, since $\log(s/\mu^2) = \log s - \log \mu^2$, and the second term is canceled thanks to the sum rule (21).

D. Similarly, for the b^4 contribution we obtain

$$F(b) = F(b=0) + F'(b=0)b^2 - \frac{b^4}{256\pi^2} \int_{4m_\pi^2}^{\infty} ds s^2 \log s \operatorname{Im} F(s) + \mathcal{O}(b^6 \log b) \quad (69)$$

valid for $F = B$ and D , where the sum rule (21) for $n = 3$ holds. The higher order terms in b contain the also $\log b$ pieces.

For J , using $K_1(b\sqrt{s}) \sim 1/(b\sqrt{s}) + b\sqrt{s}\frac{1}{4} \log(b^2 s) + \text{const} + \mathcal{O}(b^2 \log b)$, we find

$$J(b) = \frac{b^2}{16\pi^2} \int_{4m_\pi^2}^{\infty} ds s \log s \operatorname{Im} J(s) + \mathcal{O}(b^4 \log b). \quad (70)$$

Equations (68-70) are even more sensitive to the high-lying part of the spectrum than Eq. (67) due to extra powers of s in the integrand, hence the uncertainty discussed above is enhanced.

The regular behavior of $F(b=0)$ from Eq. (67) is in contrast to the case of the pion GFFs, where the long q_\perp tails (pQCD predicts $A^\pi(t) \sim D^\pi(t) \sim \alpha(t)/(-t)$ and $\Theta^\pi \sim \alpha(t)^2$ [62]) make the integrals in the Fourier transforms only conditionally convergent and thus the transverse densities of A and Θ for the pion become singular at $b = 0$ [95, 127] and of a definite sign. The appearance of this singularity is clear from the present discussion. The pion gravitational form factors A and D , as well as the pion electromagnetic form factor, have the corresponding spectral densities behaving as $\sim 1/(s \log^2 s)$. Then the integrand of (67) is asymptotically $1/(s \log s)$, which leads to divergence at $b \rightarrow 0$.

We conclude the general considerations of this subsection by remarking that for the nucleon electromagnetic form factor, $F_1(t) \sim \alpha^2/(-t)^2$, Eqs. (67,68) are valid, while for $F_2(t) \sim \alpha^2/(-t)^3$, Eq. (69) also applies.

D. Large- b asymptotics

Using Eqs. (30) for the threshold behavior of the spectral densities at the 2π branch point and formulas (65-66), we arrive at the following behavior at $b \rightarrow \infty$:

$$\begin{aligned} A(b), B(b) &\sim +e^{-2m_\pi b}/b^4, \\ J(b) &\sim +e^{-2m_\pi b}/b^3, \\ \Theta(b) &\sim +e^{-2m_\pi b}/b^2, \end{aligned} \quad (71)$$

where $+$ indicates a positive constant. The powers of b are of a kinematic origin, related to the threshold behavior. The common positive sign stems from a combination of unitarity and analyticity driven by the data analysis (see discussion in Sect. II E). The powers of b are the same as for the pion (cf. Eq. (63) of [95]), which follows from the formalism brought up in Section II E. The P-wave case of the electromagnetic form factor of the pion, using the time-like experimental data, was analyzed in [128].

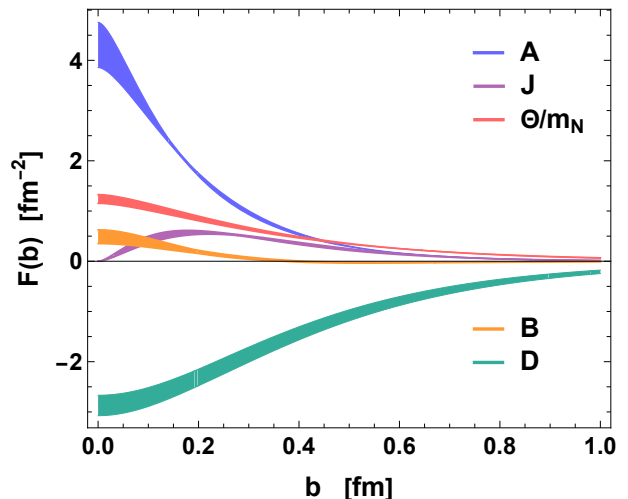


FIG. 4. Transverse densities of A , J , Θ/m_N , B , and D , plotted as functions of the transverse coordinate b , following from the meson dominance model fitted to the MIT lattice data at $m_\pi = 170$ MeV.

E. Meson dominance results

We now return to our meson dominance model. Inserting the spectral strength of the form (34) into (65) or (66) we find simple expressions involving sums of the Bessel functions $K_n(bm_i)$. The results for the basic form factors are presented in Fig. 4. For all cases, $\int 2\pi b db F(b) = F(t=0)$. The bands in the figures of this subsection indicate the errors discussed in Subsection III E, but do not include the model uncertainties discussed in Subsection IV C, as they are difficult to assess.

In [95], within a discussion for the pion, we have shown that $A(b)$ is positive definite at an operator level, i.e., independent of the hadron state in which the matrix element is taken. The present model for A complies to that general result. We note that in our model, the transverse density $A(b)$ is positive definite, as required by the positivity condition.

Classically, the angular momentum is $\mathbf{J} = \mathbf{r} \times \mathbf{p} = m \mathbf{r} \times \mathbf{v}$. Following this analogy, we define the tangential velocity profile in the nucleon as

$$v(b) = \frac{J(b)}{b\Theta(b)}. \quad (72)$$

As is seen from Fig. 5, reflecting the behavior of the involved transverse densities, $v(b)$ grows linearly from 0 at low b , reaches a maximum around 0.1 fm, and then decreases approaching 0.

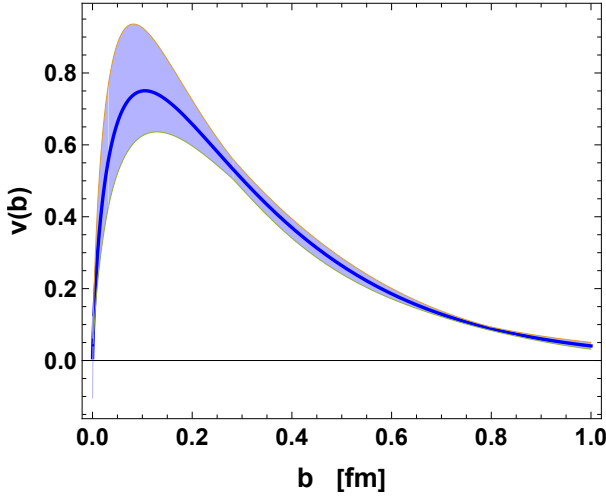


FIG. 5. Tangential velocity profile, defined in analogy to classical mechanics in Eq. (72), plotted as a function of the transverse coordinate b .

V. TRANSVERSE MECHANICAL PROPERTIES

A. Definitions and properties

The formulas displayed in this Section mirror the derivations by Polyakov and Schweitzer [122], but for the 2-dimensional transverse densities [129]. The transverse ($i, j = 1, 2$) part of SEM is

$$T^{ij}(b) = \delta^{ij}p(b) + \left(\frac{b^i b^j}{b^2} - \frac{1}{2}\delta^{ij} \right) s(b) = \quad (73)$$

$$\frac{1}{4m_N} \int \frac{d^2 q_{\perp}}{(2\pi)^2} e^{-i\mathbf{b}\cdot\mathbf{q}_{\perp}} (q_{\perp}^i q_{\perp}^j - \delta_{ij} q_{\perp}^2) D(-q_{\perp}^2).$$

The transverse pressure is therefore given by

$$p(b) = -\frac{1}{16\pi m_N} \int_0^{\infty} q_{\perp} dq_{\perp} J_0(q_{\perp} b) q_{\perp}^2 D(-q_{\perp}^2), \quad (74)$$

whereas for the stress we get

$$s(b) = -\frac{1}{8\pi m_N} \int_0^{\infty} q_{\perp} dq_{\perp} J_2(q_{\perp} b) q_{\perp}^2 D(-q_{\perp}^2). \quad (75)$$

Since $J_0(z) = 1 - z^2/4 + \dots$, at the origin the pressure is positive and concave, as long as $D(-q_{\perp}^2)$ is negative. Similarly, $J_2(z) = z^2/8 + \dots$ implies vanishing and convex stress near $b = 0$.

From Eq. (74) it is obvious that

$$\int_0^{\infty} db 2\pi b p(b) = 0, \quad (76)$$

as required by a classical analogue of the stability condition. One can also show that

$$\int_0^{\infty} db 2\pi b s(b) = -\frac{1}{2m_N} \int_0^{\infty} q_{\perp} dq_{\perp} D(-q_{\perp}^2). \quad (77)$$

From the conservation of a static SEM, $\partial/\partial b^i T^{ij} = 0$, the equation

$$p'(b) + \frac{1}{2}s'(b) + \frac{s(b)}{b} = 0 \quad (78)$$

follows. As a check, this relation can be verified with the identity between the Bessel functions, $J'_0(z) + J'_2(z) + 2J_2(z)/z = 0$, applied to Eqs. (74) and (75). Integration of (78) by parts yields

$$p(0) = \int_0^{\infty} \frac{s(b)}{b} db. \quad (79)$$

Other relations can be derived, stemming from the fact that $p(b)$ and $s(b)$ are defined via integrals with common function $D(-q_{\perp}^2)$ and the two Bessel functions:

$$\int_0^{\infty} p(b) db = \frac{1}{2} \int_0^{\infty} s(b) db,$$

$$\int_0^{\infty} b^2 p(b) db = -\frac{1}{6} \int_0^{\infty} b^2 s(b) db,$$

$$\dots \quad (80)$$

In particular, the following relation with the D -term holds:

$$D(0) = 2m_N \int_0^{\infty} 2\pi b db b^2 p(b) = -\frac{m_N}{2} \int_0^{\infty} 2\pi b db b^2 s(b). \quad (81)$$

The spectral representation is

$$p(b) = \frac{1}{16\pi^2 m_N} \int_{4m_{\pi}^2}^{\infty} ds K_0(b\sqrt{s}) s \text{Im} D(s),$$

$$s(b) = -\frac{1}{8\pi^2 m_N} \int_{4m_{\pi}^2}^{\infty} ds K_2(b\sqrt{s}) s \text{Im} D(s), \quad (82)$$

from where, in conjunction with the super-convergence sum rules, it follows that

$$p(b=0) = -\frac{1}{32\pi^2 m_N} \int_{4m_{\pi}^2}^{\infty} ds s \log s \text{Im} D(s), \quad (83)$$

$$\left. \frac{ds(b^2)}{db^2} \right|_{b=0} = \frac{1}{64\pi^2 m_N} \int_{4m_{\pi}^2}^{\infty} ds s^2 \log s \text{Im} D(s).$$

Note the sensitivity to the high- s time-like region.

The asymptotic behavior, reflecting Eq. (46) and obtained straightforwardly via Eq. (82), is

$$p(b) \sim -e^{-2m_{\pi}b}/b^2,$$

$$s(b) \sim +e^{-2m_{\pi}b}/b^2. \quad (84)$$

Note it is governed by the behavior of $\text{Im} \Theta(s)$, which is dominant at the 2π threshold.

Finally, using the fact that $2T^{+-}(b) = \epsilon(b)$ is the transverse energy density, one has the natural relation

$$\theta(b) = \epsilon(b) - 2p(b) \quad (85)$$

Note that we intuitively expect $\epsilon(b) > 0$, although $p(b)$ changes sign and $\theta(b)$ need not be positive (it was not in the pion case [95]). We have checked that indeed $\epsilon(b)$ is positive in the present meson dominance analysis.

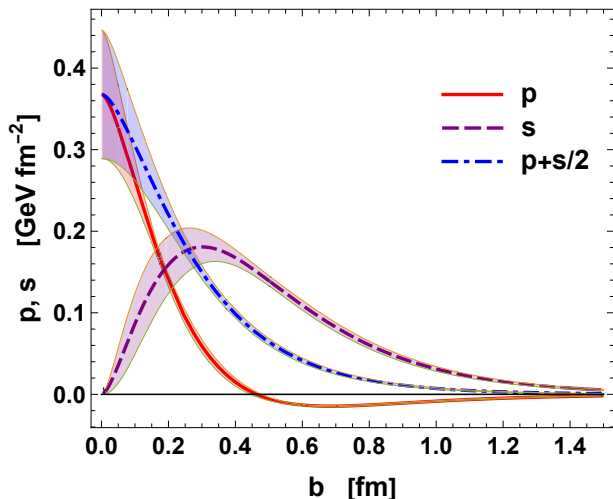


FIG. 6. Pressure p and stress s in the nucleon, evaluated in the meson dominance model fitted to the MIT lattice data at $m_\pi = 170$ MeV. The combination $p + \frac{1}{2}s$ is positive, as required by stability.

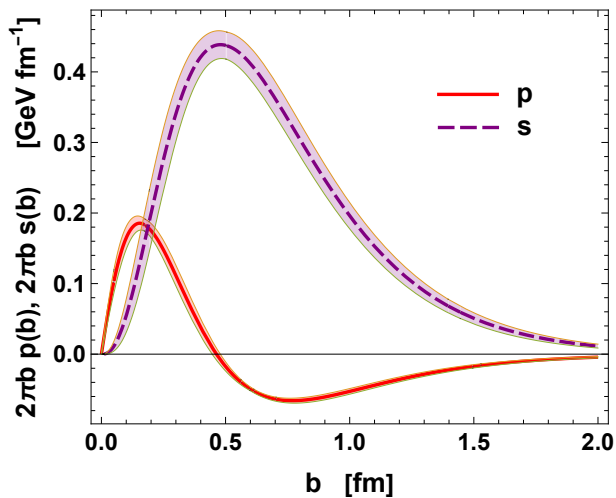


FIG. 7. Pressure p and stress s in the nucleon in the meson dominance model, multiplied with $2\pi b$. The pressure changes sign for + to - as b increases, and $\int_0^\infty 2\pi b p(b) db = 0$, as required by stability.

B. Meson dominance results

The transverse pressure and stress evaluated in the meson dominance model of the previous sections are plotted in Fig. 6. We also show the combination $p(b) + s(b)/2$, whose positivity is the local criterion for classical stability [122] for the 2-dimensional case. We see from the figure that this criterion is satisfied. In Fig. 7 we display the pressure and stress multiplied with $2\pi b$. It is clearly seen that the positive pressure inside the nucleon is compensated by the negative pressure outside, in agreement with Eq. (76) and expectations from classical stability conditions.

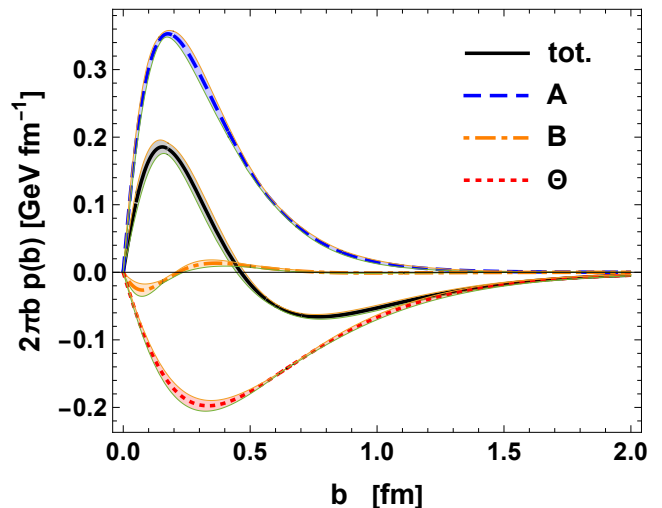


FIG. 8. Various contributions to the transverse pressure (multiplied with $2\pi b$) according to Eq. (86). The repulsive part comes from A , the confining part from Θ , and the contribution of B is small and changing the sign.

Finally, we note that the pressure can be written as

$$p(b) = \frac{m_N}{6} A(b) + \frac{1}{24m_N} \frac{1}{b} \frac{d}{db} b \frac{d}{db} B(b) - \frac{1}{6} \Theta(b). \quad (86)$$

This decomposition is shown in Fig. 8. We can see that the contribution of A , which by the general argument is positive, is repulsive and short-range, the contribution of B is small, whereas the contribution of Θ is attractive and long range. Certainly, the long range of the Θ part reflects the smallness of the σ mass, while the short range of A is associated to the larger mass of f_2 . Note that this very simple interpretation depends crucially on the proper spin decomposition of SEM introduced in Sec. II A. Qualitatively similar results were obtained in [67, 68], where the 0^{++} component is associated with the gluon contribution to the trace anomaly.

C. Transverse radii

The two-dimensional transverse radii are obtained from the densities of Sec. IV as

$$\langle b^2 \rangle_F = \frac{\int_0^\infty 2\pi b b^2 F(b)}{\int_0^\infty 2\pi b F(b)} = \frac{4}{F(0)} \left. \frac{dF(t)}{dt} \right|_{t=0}, \quad (87)$$

whereas the mechanical radius is

$$\langle b^2 \rangle_{\text{mech}} = \frac{\int_0^\infty 2\pi b b^2 [p(b) + \frac{1}{2}s(b)]}{\int_0^\infty 2\pi b [p(b) + \frac{1}{2}s(b)]} = \frac{4D(0)}{\int_0^\infty d(-t)D(t)}. \quad (88)$$

In our meson dominance model we find

$$\langle b^2 \rangle_A = 4 \left(-c_A + \frac{1}{m_{f_2}^2} + \frac{1}{m_{f_2'}^2} + \frac{1}{m_{f_2''}^2} + \frac{1}{m_{f_2'''}^2} \right) = [0.34(1) \text{ fm}]^2, \quad (89)$$

where numerically c_A approximately cancels the contribution $1/m_{f_2''}^2 + 1/m_{f_2'''}^2$. Similarly,

$$\langle b^2 \rangle_\Theta = 4 \left(\frac{1}{m_\sigma^2} + \frac{1}{m_{f_0}^2} \right) = [0.60(3) \text{ fm}]^2, \quad (90)$$

where the comparatively large size reflects the smallness of the effective σ mass. Finally,

$$\langle b^2 \rangle_{\text{mech}} = [0.48(3) \text{ fm}]^2, \quad (91)$$

with the hierarchy $\langle b^2 \rangle_A < \langle b^2 \rangle_{\text{mech}} < \langle b^2 \rangle_\Theta$.

VI. RADIAL DENSITIES

A. Definitions

For $F = A, B$, or Θ , the three-dimensional spatial distributions [122] are defined in the Breit frame as

$$F(r) = \int \frac{d^3 \Delta}{(2\pi)^3} e^{-i\Delta \cdot \mathbf{r}} F(-\Delta^2) = \frac{1}{2\pi^2} \int d\Delta \Delta^2 j_0(\Delta r) F(-\Delta^2), \quad (92)$$

where $\Delta^2 = -t$ and $j_0(z) = \sin(z)/z$ is the spherical Bessel function. We recall the statement of [129] that for the nucleon (for other spin states this does not hold [130]) the three-dimensional and the transverse distributions are connected via the Abel transform. To see this explicitly, we notice that the Abel transform of the kernel in (92) is

$$2 \int_b^\infty r \Delta \frac{j_0(\Delta r)}{\sqrt{r^2 - b^2}} dr = \pi J_0(\Delta b), \quad (93)$$

which yields (64). Therefore the ‘‘tomographic information’’ contained in the transverse densities of the nucleon describes fully the three-dimensional distributions, and vice-versa.

The case of J is a bit more involved, as the spatial distribution contains both the monopole and quadrupole terms [125],

$$J^i(r) = s^i \int \frac{d^3 \Delta}{(2\pi)^3} e^{-i\Delta \cdot \mathbf{r}} \left[J(t) + \frac{2t}{3} \frac{dJ(t)}{dt} \right]_{t=-\Delta^2} + s^j \int \frac{d^3 \Delta}{(2\pi)^3} e^{-i\Delta \cdot \mathbf{r}} (\Delta^i \Delta^j - \frac{1}{3} \delta^{ij} \Delta^2) \frac{dJ(t)}{dt} \Big|_{t=-\Delta^2}, \quad (94)$$

It can be written as

$$J^i(r) = s^i J^{\text{mon}}(r) + s^j \left(\frac{r^i r^j}{r^2} - \frac{1}{3} \delta^{ij} \right) J^{\text{quad}}(r), \quad (95)$$

where the monopole and quadrupole terms are given by

$$J^{\text{mon}}(r) = -\frac{2}{3} J^{\text{quad}}(r) = \frac{r}{6\pi^2} \int_0^\infty d\Delta \Delta^3 j_1(\Delta r) J(-\Delta^2). \quad (96)$$

Note the simple proportionality relation with the factor of $-2/3$ between the monopole and quadrupole parts, which is a generic feature when $J(t)$ is nonsingular, allowing for integration by parts.

B. Spectral representation

Using the dispersion relation (20) in (92), in analogy to (65), we get the spectral representation of the three-dimensional distributions,

$$F(r) = \frac{1}{4\pi^2} \int_{4m_\pi^2}^\infty ds \frac{e^{-r\sqrt{s}}}{r} \text{Im} F(s). \quad (97)$$

Notice as a check that the Abel transform of (97) yields (65).

Expanding $\exp(-r\sqrt{s})$ at low r and using the super-convergence sum rule (21) for $n = 1$ we get

$$F(r=0) = -\frac{1}{4\pi^2} \int_{4m_\pi^2}^\infty ds \sqrt{s} \text{Im} F(s), \quad (98)$$

which indicates an even stronger sensitivity to large s than in the two-dimensional case of (65). With the overall sign in (98), the positivity of $F(0)$ means that there are parts of the corresponding spectrum with negative strength. When Eq. (21) holds for $n = 2$, then

$$F(r) = F(r=0) - \frac{r^2}{24\pi^2} \int_{4m_\pi^2}^\infty ds s^{3/2} \text{Im} F(s) + \mathcal{O}(r^3), \quad (99)$$

and additionally with $n = 3$

$$F(r) = F(r=0) + F'(r=0)r^2 + \frac{r^4}{480\pi^2} \int_{4m_\pi^2}^\infty ds s^{5/2} \text{Im} F(s) + \mathcal{O}(r^5). \quad (100)$$

For the monopole angular momentum form factor

$$J^{\text{mon}}(r) = \frac{1}{12\pi^2} \int_{4m_\pi^2}^\infty ds \frac{e^{-r\sqrt{s}}(r\sqrt{s} + 1)}{r} \text{Im} J(s). \quad (101)$$

With the super-convergence sum rules, the lowest term in the low- r expansion is

$$J^{\text{mon}}(r) = \frac{r^2}{36\pi^2} \int_{4m_\pi^2}^\infty ds s^{3/2} \text{Im} J(s) + \mathcal{O}(r^3). \quad (102)$$

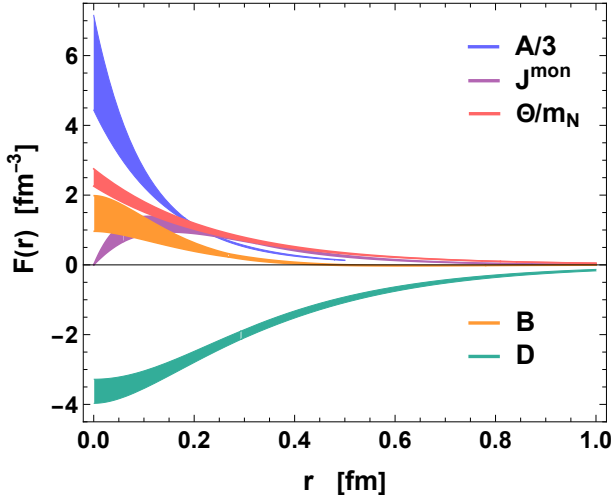


FIG. 9. Three-dimensional distributions of A (divided by 3), J^{mon} , Θ/m_N , B , and D , plotted as functions of the radial coordinate r , following from the meson dominance model fitted to the MIT lattice data at $m_\pi = 170$ MeV.

C. Radial pressure and shear forces

From the form of (98-100,102), we expect the three-dimensional distributions near the origin to be sensitive to the details of the high- s spectrum, hence to the particular model used. This is the same issue that occurred in the transverse densities, but now the model dependence is even stronger.

In Fig. 9 we plot the three-dimensional densities for the nucleon from the meson dominance model. We note that at the origin they have a large uncertainty, as discussed above. The density $A(r)$ is the largest, as the corresponding form factor has a longest tail in $-t$, caused by the large values of the tensor meson masses. Except for $B(r)$, which changes the sign, all the other densities have a definite sign.

The three-dimensional pressure and shear are evaluated as [122]

$$p(r) = -\frac{1}{12\pi^2 m_N} \int d\Delta \Delta^4 j_0(\Delta r) D(-\Delta^2),$$

$$s(r) = -\frac{1}{8\pi^2 m_N} \int d\Delta \Delta^4 j_2(\Delta r) D(-\Delta^2). \quad (103)$$

They satisfy all the relations spelled out in [122], in particular $\int_0^\infty 4\pi r^2 p(r) dr = 0$ and $-m_N \int_0^\infty 4\pi r^4 p(r) dr = -\frac{4}{15} m_N \int_0^\infty 4\pi r^4 s(r) dr = D(0)$.

We plot these mechanical distributions in Fig. 11. Higher central pressure than the one obtained from the chiral soliton model [52] means that the nucleon is a spatially more compact object in the meson dominance approach. In Fig. 12 we plot $4\pi r^4 m_N p(r)$, which integrates to $D(0)$.

Using the same methods as in Section V A we get the

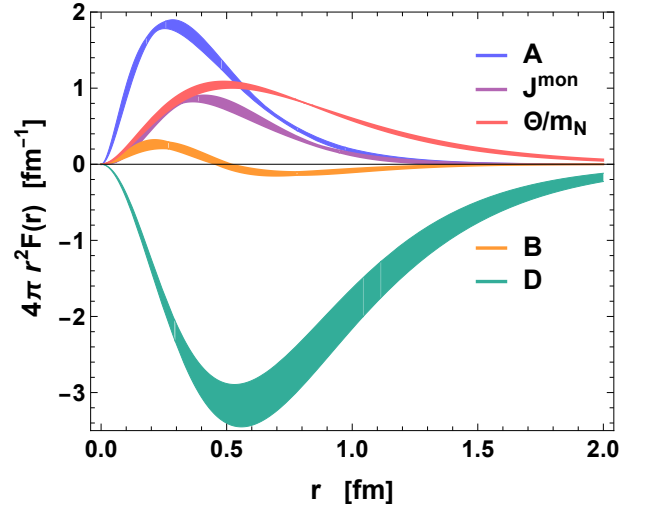


FIG. 10. Radial densities of A , J^{mon} , Θ/m_N , B , and D , plotted as functions of the radial coordinate r , following from the meson dominance model fitted to the MIT lattice data at $m_\pi = 170$ MeV.

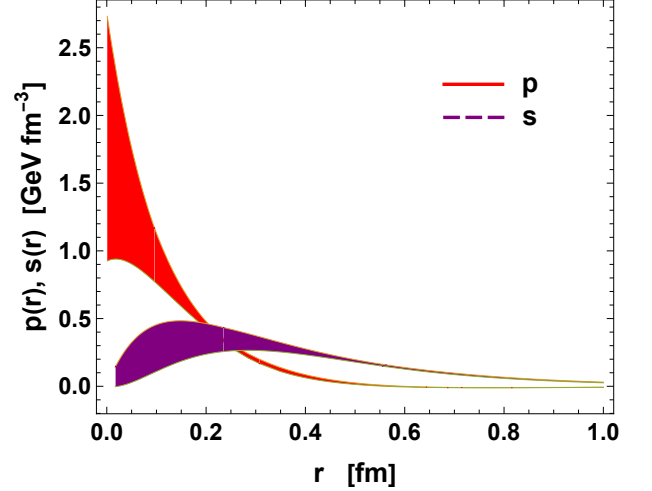


FIG. 11. Same as in Fig. 9 but for the pressure and stress. The pressure changes sign from + to - as r increases, at $r \simeq 0.5$ fm, and $\int_0^\infty 4\pi r^2 p(r) dr = 0$, as required by stability.

sum rules

$$p(r=0) = -\frac{1}{24\pi^2 m_N} \int_{4m_\pi^2}^\infty ds s^{3/2} \text{Im} D(s), \quad (104)$$

$$\left. \frac{ds(r)}{dr^2} \right|_{r=0} = \frac{1}{240\pi^2 m_N} \int_{4m_\pi^2}^\infty ds s^{5/2} \text{Im} D(s).$$

The large- r asymptotics at $r \rightarrow \infty$, following from the threshold behavior of Eq. (46), is

$$p(r) \sim -e^{-2m_\pi r} / r^{5/2},$$

$$s(r) \sim +e^{-2m_\pi r} / r^{5/2}, \quad (105)$$

where the tail of $\Theta(r) \sim +e^{-2m_\pi r} / r^{5/2}$ determines the falloff. For completeness, we mention that $A(r), B(r) \sim$

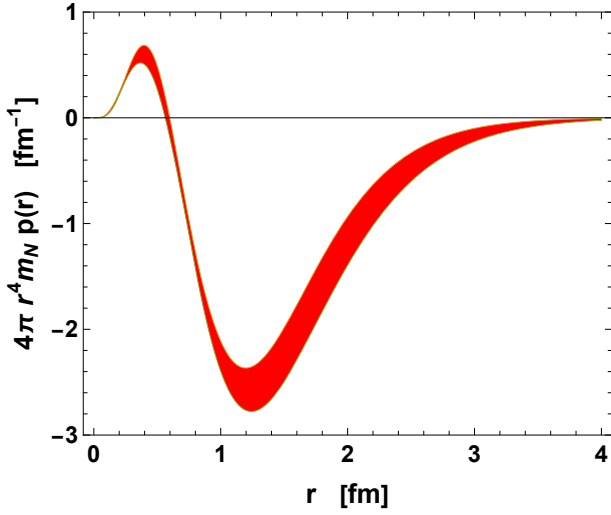


FIG. 12. Same as in Fig. 11 but for the pressure multiplied with $4\pi r^4 m_N$, which upon integration yields $D(0)$.

$+e^{-2m_\pi r}/r^{9/2}$ and $J^{\text{mon}}(r) \sim +e^{-2m_\pi r}/r^{7/2}$. We notice that the power of $1/r$ in the tails of Eq. (105) differs from the result obtained in the Chiral Soliton model [52], where the falloff was faster, $\sim e^{-2m_\pi r}/r^6$. This is probably caused by the large- N_c limit taken first in that approach. Our asymptotics robustly reflects the kinematic behavior at the 2π production threshold.

D. Radii and the D -term

The three-dimensional mean squared radii are

$$\langle r^2 \rangle_F = \frac{\int d^3r r^2 F(r)}{\int d^3r F(r)} = \frac{6}{F(0)} \left. \frac{dF(t)}{dt} \right|_{t=0}. \quad (106)$$

In our meson dominance model

$$\langle r^2 \rangle_A = 6 \left(-c_A + \frac{1}{m_{f_2}^2} + \frac{1}{m_{f_2'}^2} + \frac{1}{m_{f_2''}^2} + \frac{1}{m_{f_2'''}^2} \right) = [0.51(1) \text{ fm}]^2, \quad (107)$$

and

$$\langle r^2 \rangle_\Theta = 6 \left(\frac{1}{m_\sigma^2} + \frac{1}{m_{f_0}^2} \right) = [0.90(4) \text{ fm}]^2. \quad (108)$$

For the angular momentum density

$$\langle r^2 \rangle_J = \frac{\int d^3r r^2 J^i(r)}{\int d^3r J^i(r)} = \frac{10}{J(0)} \left. \frac{dJ(t)}{dt} \right|_{t=0} = 20 \left. \frac{dJ(t)}{dt} \right|_{t=0}, \quad (109)$$

with only the monopole term contributing. In the meson dominance model

$$\langle r^2 \rangle_J = 10 \left(-c_J + \frac{1}{m_{f_2}^2} + \frac{1}{m_{f_2'}^2} + \frac{1}{m_{f_2''}^2} + \frac{1}{m_{f_2'''}^2} \right) = [0.57(3) \text{ fm}]^2. \quad (110)$$

The D -term is related to the mean square radii as follows:

$$D(0) = \frac{2m_N^2}{9} (\langle r^2 \rangle_A - \langle r^2 \rangle_\Theta). \quad (111)$$

The mechanical radius, as defined in [122], is

$$\langle r^2 \rangle_{\text{mech}} = \frac{6D(0)}{\int_0^\infty d(-t)D(t)} = [0.72(5) \text{ fm}]^2, \quad (112)$$

and the energy radius, defined via T^{00} [122], is

$$\langle r^2 \rangle_E = \langle r^2 \rangle_A - \frac{3}{2m_N^2} D(0) = \frac{2}{3} \langle r^2 \rangle_A + \frac{1}{3} \langle r^2 \rangle_\Theta = [0.67(2) \text{ fm}]^2 \quad (113)$$

(cf. various estimates for $\langle r^2 \rangle_{\text{mass}} \equiv \langle r^2 \rangle_E$ collected in [123]). To summarize, we find the hierarchy

$$\langle r^2 \rangle_A < \langle r^2 \rangle_J < \langle r^2 \rangle_E < \langle r^2 \rangle_{\text{mech}} < \langle r^2 \rangle_\Theta, \quad (114)$$

spanning the sizes from 0.5 fm to 0.9 fm. Note that the largest value of $\langle r^2 \rangle_\Theta$ reflects the fact that the trace-anomaly lattice from factor of Fig. 2 is the shortest-range, hence has the highest slope at the origin, essentially reflecting the smallness of the effective σ mass. This is in contrast to the extraction by Kharzeev [73] from the GlueX J/ψ photoproduction data [71], where a relatively small value of $\langle r^2 \rangle_\Theta \sim [0.55 \text{ fm}]^2$ was found (see also the discussion in [74, 75]).

VII. CONCLUSIONS

In this paper we have discussed several general issues concerning GFFs of the nucleon and its mechanical properties, involving dispersion relations, super-convergence sum rules, asymptotic behavior, or positivity, as well as offered a natural fit of the available lattice data within the meson dominance approach.

On the general grounds, GFFs of the nucleon can be scrutinized from the point of view analyticity realized through the established long ago meson dominance principle, and implemented through the pertinent current-field identities. While GFFs are admittedly complicated structures for the time-like momenta, displaying resonance profiles corresponding to the exchanged mesons and the corresponding backgrounds, the space-like region, which has been lately the main concern both for the theory and experiment, is largely independent of these details. We have shown that the meson dominance

works well for the lattice QCD data for the nucleon in the available space-like domain, mirroring the success for the pion [93].

Since the pQCD constraints impose known power falloffs based on the leading two gluon exchange process, $A, J \sim \alpha^2/(-t)^2$, $B, D \sim \alpha^2/(-t)^3$, these requirements have been incorporated into our model in terms of a minimum number of resonances. The Q^2 range covered by the lattice QCD simulation, $0 \leq Q^2 \leq 2 \text{ GeV}^2$, does not probe precisely the asymptotics fall-off, therefore the corresponding super-convergence sum rules or the spectral representation of the spatial densities, are only weakly constrained by the present data.

Estimates for various radii, exhibiting a certain hierarchy, and for the value of the D -term, have been made within the meson dominance model. A large value of the mass (trace-anomaly) radius, reflecting the smallness of the effective σ mass, has been found from the fit. A very similar best fit value, $m_\sigma \sim 0.65 \text{ GeV}$, has been found for both the pion and the nucleon.

For the spatial distributions, we have derived sum rules for their values and derivatives at the origin in terms of the spectral integrals with the application of the super-convergence sum rules. We argue that these quantities are weakly constrained, since we do not have sufficient knowledge on the corresponding spectral strengths.

From the threshold behavior in the time-like region for the $\pi\pi \rightarrow N\bar{N}$, using Watson's theorem, we have derived the leading asymptotic behavior at large values of the coordinate for the spatial densities, including the pressure and shear forces. These formulas involve the obvious two-pion Yukawa tail, multiplied with a power falloff. The formulas obtained from our study exhibit the signs following from the $\pi-N$ elastic scattering data, which are positive for all the considered densities, except for the pressure, where the coefficient is negative.

The decomposition of SEM into the 0^{++} and 2^{++} part offers a natural explanation of the spatial variance of pressure, whose attractive tail is associated with the small mass of the σ meson, while the inside repulsion is due to the large mass of the f_2 meson.

We also bring up the result [95] that the transverse distribution related to the T^{++} is positive at an operator level. This implies in general that $A(b) > 0$, which is

satisfied in our model.

We are grateful to the authors of Ref. [79] and [84] for sending us the numbers for their lattice results. One of us (ERA) thanks Christian Weiss for clarifications regarding the positivity conditions.

ERA was supported by Spanish MINECO and European FEDER funds grant and by Project No. PID2023-147072NB-I00 funded by MCIN/AEI/10.13039-501100011033, and by the Junta de Andalucía grant FQM-225.

Appendix A: Features of the minimum meson dominance ansatz

Expansion of the meson-dominance function for $A(t)$ from Eq. (48) at low t yields

$$A(t) = 1 + St + Rt^2 + \mathcal{O}(t^3), \quad (\text{A1})$$

with

$$S = -c_A + \frac{1}{m_{f_2}^2} + \frac{1}{m_{f_2'}^2} + \frac{1}{m_{f_2''}^2} + \frac{1}{m_{f_2'''}^2}, \quad (\text{A2})$$

$$R = c_2 - \frac{c_A^2}{2} + \frac{1}{2} \left(\frac{1}{m_{f_2}^4} + \frac{1}{m_{f_2'}^4} + \frac{1}{m_{f_2''}^4} + \frac{1}{m_{f_2'''}^4} + S^2 \right).$$

Thus, for a given set of the four resonance masses, c_A and c_2 can be adjusted to fit the slope and the curvature of the function at the origin. At asymptotically large $-t$,

$$A(t) = \frac{c_2 m_{f_2}^2 m_{f_2'}^2 m_{f_2''}^2 m_{f_2'''}^2}{(-t)^2} + \mathcal{O}[1/(-t)^3]. \quad (\text{A3})$$

Analogous formulas hold for $J(t)$.

For $B(t)$ we have the features

$$B(t) = (c_A - c_J) \left[t + \left(\frac{1}{m_{f_2}^2} + \frac{1}{m_{f_2'}^2} + \frac{1}{m_{f_2''}^2} + \frac{1}{m_{f_2'''}^2} \right) t^2 \right] + \mathcal{O}(t^3), \quad (\text{A4})$$

and

$$B(t) = \frac{(c_J - c_A) m_{f_2}^2 m_{f_2'}^2 m_{f_2''}^2 m_{f_2'''}^2}{(-t)^3} + \mathcal{O}[1/(-t)^4]. \quad (\text{A5})$$

-
- [1] E. E. Chambers and R. Hofstadter, "Structure of the Proton," *Phys. Rev.* **103**, 1454–1463 (1956).
 - [2] SD Drell, F Zachariasen, and Eugene Guth, "Electromagnetic structure of nucleons," (1962).
 - [3] William R. Frazer and Jose R. Fulco, "Effect of a pion pion scattering resonance on nucleon structure," *Phys. Rev. Lett.* **2**, 365 (1959).
 - [4] William R. Frazer and Jose R. Fulco, "Partial-Wave Dispersion Relations for the Process $\pi\pi \rightarrow N\bar{N}$," *Phys.*

- Rev.* **117**, 1603–1609 (1960).
- [5] William R. Frazer and Jose R. Fulco, "Effect of a Pion-Pion Scattering Resonance on Nucleon Structure. II," *Phys. Rev.* **117**, 1609–1614 (1960).
- [6] J. J. Sakurai, "Theory of strong interactions," *Annals Phys.* **11**, 1–48 (1960).
- [7] T. D. Lee and B. Zumino, "Field Current Identities and Algebra of Fields," *Phys. Rev.* **163**, 1667–1681 (1967).
- [8] N. M. Kroll, T. D. Lee, and B. Zumino, "Neutral Vec-

- tor Mesons and the Hadronic Electromagnetic Current,” *Phys. Rev.* **157**, 1376–1399 (1967).
- [9] R. G. Sachs, “High-Energy Behavior of Nucleon Electromagnetic Form Factors,” *Phys. Rev.* **126**, 2256–2260 (1962).
- [10] Gordon N. Fleming, “Charge Distributions from Relativistic Form-Factors,” in *Physical reality and mathematical description: Festschrift Jauch (Josef Maria) on his 60th birthday*, edited by Charles P. Enz and Jagdish Mehra (1974) pp. 357–374.
- [11] Davison E. Soper, “Parton model and the bethe-salpeter wave function,” *Phys. Rev. D* **15**, 1141–1149 (1977).
- [12] Matthias Burkardt, “Impact parameter dependent parton distributions and off forward parton distributions for $\zeta \rightarrow 0$,” *Phys. Rev. D* **62**, 071503 (2000), [Erratum: *Phys.Rev.D* 66, 119903 (2002)], arXiv:hep-ph/0005108.
- [13] M. Diehl, “Generalized parton distributions in impact parameter space,” *Eur. Phys. J. C* **25**, 223–232 (2002), [Erratum: *Eur.Phys.J.C* 31, 277–278 (2003)], arXiv:hep-ph/0205208.
- [14] Matthias Burkardt, “Impact parameter space interpretation for generalized parton distributions,” *Int. J. Mod. Phys. A* **18**, 173–208 (2003), arXiv:hep-ph/0207047.
- [15] Gerald A. Miller, “Transverse Charge Densities,” *Ann. Rev. Nucl. Part. Sci.* **60**, 1–25 (2010), arXiv:1002.0355 [nucl-th].
- [16] Adam Freese and Gerald A. Miller, “Convolution formalism for defining densities of hadrons,” *Phys. Rev. D* **108**, 034008 (2023), arXiv:2210.03807 [hep-ph].
- [17] P. V. Pobylitsa, “Positivity bounds on generalized parton distributions in impact parameter representation,” *Phys. Rev. D* **66**, 094002 (2002), hep-ph/0204337.
- [18] I. Yu. Kobzarev and L. B. Okun, “Gravitational interaction of fermions,” *Zh. Eksp. Teor. Fiz.* **43**, 1904–1909 (1962).
- [19] P GO Freund, ““ universality” and high energy total cross sections,” *Phys. Letters* **2** (1962).
- [20] David H. Sharp and William G. Wagner, “Asymptotic Behavior of Nucleon-Nucleon Scattering,” *Phys. Rev.* **131**, 2226–2238 (1963).
- [21] Heinz Pagels, “Energy-momentum structure form factors of particles,” *Phys. Rev.* **144**, 1250–1260 (1966).
- [22] Julian Schwinger, “Field Theory of Matter. 4.” *Phys. Rev.* **140**, B158–B163 (1965).
- [23] Robert Delbourgo, Abdus Salam, and J. A. Strathdee, “The stress tensor and the 2+ mesons,” *Nuovo Cim.* **49**, 593–605 (1967).
- [24] W. Królikowski, “Partial conservation and the 2+ mesons,” *Phys. Lett. B* **24**, 305–306 (1967).
- [25] K. Raman, “Spin-two mesons, the stress tensor, and a field-source identity. i,” (1970).
- [26] K. Raman, “Some consequences of tensor-meson dominance,” *Phys. Rev. D* **3**, 2900–2906 (1971).
- [27] Sharashchandra H Patil and York-Peng Yao, “Universality principles with 1- and 2+ dominance,” *Physical Review* **153**, 1455 (1967).
- [28] C. J. Isham, Abdus Salam, and J. A. Strathdee, “F-dominance of gravity,” *Phys. Rev. D* **3**, 867–873 (1971).
- [29] M. G. Hare and G. Papini, “Mass radius of the nucleon,” *Can. J. Phys.* **50**, 1163–1168 (1972).
- [30] Xiang-Dong Ji, “Deeply virtual Compton scattering,” *Phys. Rev. D* **55**, 7114–7125 (1997), arXiv:hep-ph/9609381.
- [31] Maxim V. Polyakov and C. Weiss, “Skewed and double distributions in pion and nucleon,” *Phys. Rev. D* **60**, 114017 (1999), arXiv:hep-ph/9902451.
- [32] M. V. Polyakov, “Generalized parton distributions and strong forces inside nucleons and nuclei,” *Phys. Lett. B* **555**, 57–62 (2003), arXiv:hep-ph/0210165.
- [33] Cédric Lorcé, Hervé Moutarde, and Arkadiusz P. Trawiński, “Revisiting the mechanical properties of the nucleon,” *Eur. Phys. J. C* **79**, 89 (2019), arXiv:1810.09837 [hep-ph].
- [34] Cédric Lorcé, Andreas Metz, Barbara Pasquini, and Simone Rodini, “Energy-momentum tensor in QCD: nucleon mass decomposition and mechanical equilibrium,” *JHEP* **11**, 121 (2021), arXiv:2109.11785 [hep-ph].
- [35] E. Epelbaum, J. Gegelia, N. Lange, U. G. Meißner, and M. V. Polyakov, “Definition of Local Spatial Densities in Hadrons,” *Phys. Rev. Lett.* **129**, 012001 (2022), arXiv:2201.02565 [hep-ph].
- [36] J. Yu. Panteleeva, E. Epelbaum, J. Gegelia, and U. G. Meißner, “Definition of gravitational local spatial densities for spin-0 and spin-1/2 systems,” *Eur. Phys. J. C* **83**, 617 (2023), arXiv:2211.09596 [hep-ph].
- [37] Cédric Lorcé, Peter Schweitzer, and Kemal Tezgin, “2D energy-momentum tensor distributions of nucleon in a large- N_c quark model from ultrarelativistic to non-relativistic limit,” *Phys. Rev. D* **106**, 014012 (2022), arXiv:2202.01192 [hep-ph].
- [38] X. D. Ji, “Gauge-invariant decomposition of nucleon spin,” *Phys. Rev. Lett.* **78**, 610–613 (1997), arXiv:hep-ph/9603249.
- [39] E. Leader and C. Lorcé, “The angular momentum controversy: What’s it all about and does it matter?” *Phys. Rept.* **541**, 163–248 (2014), arXiv:1309.4235 [hep-ph].
- [40] Cédric Lorcé, “On the hadron mass decomposition,” *Eur. Phys. J. C* **78**, 120 (2018), arXiv:1706.05853 [hep-ph].
- [41] Yoshitaka Hatta, Abha Rajan, and Kazuhiro Tanaka, “Quark and gluon contributions to the QCD trace anomaly,” *JHEP* **12**, 008 (2018), arXiv:1810.05116 [hep-ph].
- [42] Ho-Yeon Won and Cédric Lorcé, “Relativistic energy-momentum tensor distributions in a polarized nucleon,” (2025), arXiv:2503.07382 [hep-ph].
- [43] V. D. Burkert, L. Elouadrhiri, F. X. Girod, C. Lorcé, P. Schweitzer, and P. E. Shanahan, “Colloquium: Gravitational form factors of the proton,” *Rev. Mod. Phys.* **95**, 041002 (2023), arXiv:2303.08347 [hep-ph].
- [44] Cédric Lorcé and Peter Schweitzer, “Pressure inside hadrons: criticism, conjectures, and all that,” (2025), arXiv:2501.04622 [hep-ph].
- [45] Andrei V. Belitsky and X. Ji, “Chiral structure of nucleon gravitational form-factors,” *Phys. Lett. B* **538**, 289–297 (2002), arXiv:hep-ph/0203276.
- [46] Shung-ichi Ando, Jiunn-Wei Chen, and Chung-Wen Kao, “Leading chiral corrections to the nucleon generalized parton distributions,” *Phys. Rev. D* **74**, 094013 (2006), arXiv:hep-ph/0602200.
- [47] M. Diehl, A. Manashov, and A. Schafer, “Chiral perturbation theory for nucleon generalized parton distributions,” *Eur. Phys. J. A* **29**, 315–326 (2006), [Erratum: *Eur.Phys.J.A* 56, 220 (2020)], arXiv:hep-ph/0608113.
- [48] A. M. Moiseeva and A. A. Vladimirov, “On chiral corrections to nucleon GPD,” *Eur. Phys. J. A* **49**, 23 (2013), arXiv:1208.1714 [hep-ph].
- [49] Marina Dorati, Tobias A. Gail, and Thomas R. Hem-

- mert, “Chiral perturbation theory and the first moments of the generalized parton distributions in a nucleon,” *Nucl. Phys. A* **798**, 96–131 (2008), arXiv:nucl-th/0703073.
- [50] H. Alharazin, D. Djukanovic, J. Gegelia, and M. V. Polyakov, “Chiral theory of nucleons and pions in the presence of an external gravitational field,” *Phys. Rev. D* **102**, 076023 (2020), arXiv:2006.05890 [hep-ph].
- [51] K. Goeke, Maxim V. Polyakov, and M. Vanderhaeghen, “Hard exclusive reactions and the structure of hadrons,” *Prog. Part. Nucl. Phys.* **47**, 401–515 (2001), arXiv:hep-ph/0106012.
- [52] K. Goeke, J. Grabis, J. Ossmann, M. V. Polyakov, P. Schweitzer, A. Silva, and D. Urbano, “Nucleon form-factors of the energy momentum tensor in the chiral quark-soliton model,” *Phys. Rev. D* **75**, 094021 (2007), arXiv:hep-ph/0702030.
- [53] C. Cebulla, K. Goeke, J. Ossmann, and P. Schweitzer, “The Nucleon form-factors of the energy momentum tensor in the Skyrme model,” *Nucl. Phys. A* **794**, 87–114 (2007), arXiv:hep-ph/0703025.
- [54] Matt J. Neubelt, Andrew Sampino, Jonathan Hudson, Kemal Tezgin, and Peter Schweitzer, “Energy momentum tensor and the D-term in the bag model,” *Phys. Rev. D* **101**, 034013 (2020), arXiv:1911.08906 [hep-ph].
- [55] Zainul Abidin and Carl E. Carlson, “Nucleon electromagnetic and gravitational form factors from holography,” *Phys. Rev. D* **79**, 115003 (2009), arXiv:0903.4818 [hep-ph].
- [56] Chandan Mondal, “Longitudinal momentum densities in transverse plane for nucleons,” *Eur. Phys. J. C* **76**, 74 (2016), arXiv:1511.01736 [hep-ph].
- [57] Jiali Deng and Defu Hou, “The nucleon structure from an AdS/QCD model in the Veneziano limit,” (2025), arXiv:2502.00771 [nucl-th].
- [58] I. V. Anikin, “Gravitational form factors within light-cone sum rules at leading order,” *Phys. Rev. D* **99**, 094026 (2019), arXiv:1902.00094 [hep-ph].
- [59] K. Azizi and U. Özdem, “Nucleon’s energy–momentum tensor form factors in light-cone QCD,” *Eur. Phys. J. C* **80**, 104 (2020), arXiv:1908.06143 [hep-ph].
- [60] Sreeraj Nair, Chandan Mondal, Siqi Xu, Xingbo Zhao, Asmita Mukherjee, and James P. Vary (BLFQ), “Gravitational form factors and mechanical properties of quarks in protons: A basis light-front quantization approach,” *Phys. Rev. D* **110**, 056027 (2024), arXiv:2403.11702 [hep-ph].
- [61] Siqi Xu, Yiping Liu, Chandan Mondal, Jiangshan Lan, Xingbo Zhao, Yang Li, and James P. Vary, “Towards a first principles light-front Hamiltonian for the nucleon,” (2024), arXiv:2408.11298 [hep-ph].
- [62] Xuan-Bo Tong, Jian-Ping Ma, and Feng Yuan, “Gluon gravitational form factors at large momentum transfer,” *Phys. Lett. B* **823**, 136751 (2021), arXiv:2101.02395 [hep-ph].
- [63] Xuan-Bo Tong, Jian-Ping Ma, and Feng Yuan, “Perturbative calculations of gravitational form factors at large momentum transfer,” *JHEP* **10**, 046 (2022), arXiv:2203.13493 [hep-ph].
- [64] Zeinab Dehghan, F. Almaksusi, and K. Azizi, “Mechanical properties of proton using flavor-decomposed gravitational form factors,” (2025), arXiv:2502.16689 [hep-ph].
- [65] Mitsutoshi Fujita, Yoshitaka Hatta, Shigeki Sugimoto, and Takahiro Ueda, “Nucleon D-term in holographic quantum chromodynamics,” *PTEP* **2022**, 093B06 (2022), arXiv:2206.06578 [hep-th].
- [66] Xiaobin Wang, Zanbin Xing, Minghui Ding, Khépani Raya, and Lei Chang, “Bridging Electromagnetic and Gravitational Form Factors: Insights from LFHQCD,” (2024), arXiv:2406.09644 [hep-ph].
- [67] Xiangdong Ji and Chen Yang, “Momentum Flow and Forces on Quarks in the Nucleon,” (2025), arXiv:2503.01991 [hep-ph].
- [68] Daisuke Fujii, Mamiya Kawaguchi, and Mitsuru Tanaka, “Dominance of gluonic scale anomaly in confining pressure inside nucleon and D-term,” (2025), arXiv:2503.09686 [hep-ph].
- [69] H. S. Jo *et al.* (CLAS), “Cross sections for the exclusive photon electroproduction on the proton and Generalized Parton Distributions,” *Phys. Rev. Lett.* **115**, 212003 (2015), arXiv:1504.02009 [hep-ex].
- [70] V. D. Burkert, L. Elouadrhiri, and F. X. Girod, “The pressure distribution inside the proton,” *Nature* **557**, 396–399 (2018).
- [71] A. Ali *et al.* (GlueX), “First Measurement of Near-Threshold J/ψ Exclusive Photoproduction off the Proton,” *Phys. Rev. Lett.* **123**, 072001 (2019), arXiv:1905.10811 [nucl-ex].
- [72] Xiao-Yun Wang, Fancong Zeng, and Quanjin Wang, “Systematic analysis of the proton mass radius based on photoproduction of vector charmoniums,” *Phys. Rev. D* **105**, 096033 (2022), arXiv:2204.07294 [hep-ph].
- [73] Dmitri E. Kharzeev, “Mass radius of the proton,” *Phys. Rev. D* **104**, 054015 (2021), arXiv:2102.00110 [hep-ph].
- [74] Meng-Lin Du, Vadim Baru, Feng-Kun Guo, Christoph Hanhart, Ulf-G Meißner, Alexey Nefediev, and Igor Strakovsky, “Deciphering the mechanism of near-threshold J/ψ photoproduction,” *Eur. Phys. J. C* **80**, 1053 (2020), arXiv:2009.08345 [hep-ph].
- [75] D. Winney *et al.* (Joint Physics Analysis Center), “Dynamics in near-threshold J/ψ photoproduction,” *Phys. Rev. D* **108**, 054018 (2023), arXiv:2305.01449 [hep-ph].
- [76] Muhammad Goharipour, Hadi Hashamipour, H. Fatehi, Fatemeh Irani, K. Azizi, and S. V. Goloskokov (MMGPDs), “Mechanical properties of the nucleon from the generalized parton distributions,” (2025), arXiv:2501.16257 [hep-ph].
- [77] Kiminad A. Mamo and Ismail Zahed, “ J/ψ near threshold in holographic QCD: A and D gravitational form factors,” *Phys. Rev. D* **106**, 086004 (2022), arXiv:2204.08857 [hep-ph].
- [78] Yuxun Guo, Feng Yuan, and Wenbin Zhao, “Bayesian Inferring Nucleon’s Gravitation Form Factors via Near-threshold J/ψ Photoproduction,” (2025), arXiv:2501.10532 [hep-ph].
- [79] Daniel C. Hackett, Dimitra A. Pefkou, and Phiala E. Shanahan, “Gravitational Form Factors of the Proton from Lattice QCD,” *Phys. Rev. Lett.* **132**, 251904 (2024), arXiv:2310.08484 [hep-lat].
- [80] Daniel C. Hackett, Patrick R. Oare, Dimitra A. Pefkou, and Phiala E. Shanahan, “Gravitational form factors of the pion from lattice QCD,” (2023), arXiv:2307.11707 [hep-lat].
- [81] M. Deka *et al.*, “Lattice study of quark and glue momenta and angular momenta in the nucleon,” *Phys. Rev. D* **91**, 014505 (2015), arXiv:1312.4816 [hep-lat].

- [82] P. E. Shanahan and W. Detmold, “Gluon gravitational form factors of the nucleon and the pion from lattice QCD,” *Phys. Rev. D* **99**, 014511 (2019), arXiv:1810.04626 [hep-lat].
- [83] Joseph Delmar, Constantia Alexandrou, Simone Bacchio, Ian Cloët, Martha Constantinou, and Gianinis Koutsou, “Generalized form factors of the pion and kaon using twisted mass fermions,” in *40th International Symposium on Lattice Field Theory (2024)* arXiv:2401.04080 [hep-lat].
- [84] Bigeng Wang, Fangcheng He, Gen Wang, Terrence Draper, Jian Liang, Keh-Fei Liu, and Yi-Bo Yang (χ QCD), “Trace anomaly form factors from lattice QCD,” *Phys. Rev. D* **109**, 094504 (2024), arXiv:2401.05496 [hep-lat].
- [85] Philipp Hagler, John W. Negele, Dru Bryant Renner, W. Schroers, T. Lippert, and K. Schilling (LHPC, SESAM), “Moments of nucleon generalized parton distributions in lattice QCD,” *Phys. Rev. D* **68**, 034505 (2003), arXiv:hep-lat/0304018.
- [86] M. Gockeler, R. Horsley, D. Pleiter, Paul E. L. Rakow, A. Schafer, G. Schierholz, and W. Schroers (QCDSF), “Generalized parton distributions from lattice QCD,” *Phys. Rev. Lett.* **92**, 042002 (2004), arXiv:hep-ph/0304249.
- [87] Dirk Brommel *et al.* (QCDSF-UKQCD), “Moments of generalized parton distributions and quark angular momentum of the nucleon,” *PoS LATTICE2007*, 158 (2007), arXiv:0710.1534 [hep-lat].
- [88] Philipp Hagler, “Progress in hadron structure physics on the lattice,” *PoS LATTICE2007*, 013 (2007), arXiv:0711.0819 [hep-lat].
- [89] Ph. Hagler *et al.* (LHPC), “Nucleon Generalized Parton Distributions from Full Lattice QCD,” *Phys. Rev. D* **77**, 094502 (2008), arXiv:0705.4295 [hep-lat].
- [90] J. D. Bratt *et al.* (LHPC), “Nucleon structure from mixed action calculations using 2+1 flavors of asqtad sea and domain wall valence fermions,” *Phys. Rev. D* **82**, 094502 (2010), arXiv:1001.3620 [hep-lat].
- [91] Franz Gross *et al.*, “50 Years of Quantum Chromodynamics,” *Eur. Phys. J. C* **83**, 1125 (2023), arXiv:2212.11107 [hep-ph].
- [92] Pere Masjuan, Enrique Ruiz Arriola, and Wojciech Broniowski, “Meson dominance of hadron form factors and large- N_c phenomenology,” *Phys. Rev. D* **87**, 014005 (2013), arXiv:1210.0760 [hep-ph].
- [93] Wojciech Broniowski and Enrique Ruiz Arriola, “Gravitational form factors of the pion and meson dominance,” *Phys. Lett. B* **859**, 139138 (2024), arXiv:2405.07815 [hep-ph].
- [94] Enrique Ruiz Arriola and Wojciech Broniowski, “Scalar and tensor meson dominance and gravitational form factors of the pion,” (2024) arXiv:2411.10354 [hep-ph].
- [95] Wojciech Broniowski and Enrique Ruiz Arriola, “Transverse densities of the energy-momentum tensor and the gravitational form factors the pion,” (2024) arXiv:2412.00848 [hep-ph].
- [96] Xiong-Hui Cao, Feng-Kun Guo, Qu-Zhi Li, and De-Liang Yao, “Precise Determination of Nucleon Gravitational Form Factors,” (2024), arXiv:2411.13398 [hep-ph].
- [97] John C. Collins, Anthony Duncan, and Satish D. Joglekar, “Trace and Dilatation Anomalies in Gauge Theories,” *Phys. Rev. D* **16**, 438–449 (1977).
- [98] S. Pokorski, *Gauge field theories* (Cambridge University Press, 2005).
- [99] A. V. Belitsky and A. V. Radyushkin, “Unraveling hadron structure with generalized parton distributions,” *Phys. Rept.* **418**, 1–387 (2005), hep-ph/0504030.
- [100] K. Raman, “Gravitational form-factors of pseudoscalar mesons, stress-tensor-current commutation relations, and deviations from tensor- and scalar-meson dominance,” *Phys. Rev. D* **4**, 476–488 (1971).
- [101] V. M. Braun, A. Lenz, and M. Wittmann, “Nucleon Form Factors in QCD,” *Phys. Rev. D* **73**, 094019 (2006), arXiv:hep-ph/0604050.
- [102] C. Alvegard and R. Kogerler, “Asymptotic behavior of weak form-factors within QCD,” *Z. Phys. C* **2**, 173 (1979).
- [103] Stanley J. Brodsky, G. Peter Lepage, and S. A. A. Zaidi, “Weak and Electromagnetic Form-factors of Baryons at Large Momentum Transfer,” *Phys. Rev. D* **23**, 1152 (1981).
- [104] P. Mergell, Ulf G. Meissner, and D. Drechsel, “Dispersion theoretical analysis of the nucleon electromagnetic form-factors,” *Nucl. Phys. A* **596**, 367–396 (1996), arXiv:hep-ph/9506375.
- [105] John F. Donoghue and Euy Soo Na, “Asymptotic limits and structure of the pion form factor,” *Phys. Rev.* **D56**, 7073–7076 (1997), arXiv:hep-ph/9611418.
- [106] M. A. Belushkin, H. W. Hammer, and U. G. Meissner, “Dispersion analysis of the nucleon form-factors including meson continua,” *Phys. Rev. C* **75**, 035202 (2007), arXiv:hep-ph/0608337.
- [107] R. Koch and E. Pietarinen, “Low-Energy π N Partial Wave Analysis,” *Nucl. Phys. A* **336**, 331–346 (1980).
- [108] Gerhard Höhler, *Pion-Nukleon-Streuung: Methoden und Ergebnisse phänomenologischer Analysen* (Springer, 1983).
- [109] Martin Hoferichter, Jacobo Ruiz de Elvira, Bastian Kubis, and Ulf-G. Meißner, “Roy–Steiner-equation analysis of pion–nucleon scattering,” *Phys. Rept.* **625**, 1–88 (2016), arXiv:1510.06039 [hep-ph].
- [110] D. Toublan, “Lowest tensor-meson resonances contributions to the chiral perturbation theory low energy coupling constants,” *Phys. Rev.* **D53**, 6602–6607 (1996), arXiv:hep-ph/9509217.
- [111] G. Ecker and C. Zauner, “Tensor meson exchange at low energies,” *Eur. Phys. J.* **C52**, 315–323 (2007), arXiv:0705.0624 [hep-ph] [hep-ph].
- [112] M. M Nagels *et al.*, “Compilation of Coupling Constants and Low-Energy Parameters. 1976 Edition,” *Nucl. Phys. B* **109**, 1–90 (1976).
- [113] Michael D. Scadron, “Covariant Propagators and Vertex Functions for Any Spin,” *Phys. Rev.* **165**, 1640–1647 (1968).
- [114] Yu. V. Novozhilov, *Introduction to Elementary Particle Theory*, International Series of Monographs In Natural Philosophy (Pergamon Press, Oxford, UK, 1975).
- [115] G. J. Gounaris and J. J. Sakurai, “Finite width corrections to the vector meson dominance prediction for $\rho \rightarrow e^+e^-$,” *Phys. Rev. Lett.* **21**, 244–247 (1968).
- [116] J. P. Lees *et al.* (BaBar), “Precise Measurement of the $e^+e^- \rightarrow \pi^+\pi^-(\gamma)$ Cross Section with the Initial-State Radiation Method at BABAR,” *Phys. Rev. D* **86**, 032013 (2012), arXiv:1205.2228 [hep-ex].
- [117] S. Navas *et al.* (Particle Data Group), “Review of particle physics,” *Phys. Rev. D* **110**, 030001 (2024).

- [118] L. Alvarez-Ruso, T. Ledwig, J. Martin Camalich, and M. J. Vicente-Vacas, “Nucleon mass and pion-nucleon sigma term from a chiral analysis of lattice QCD data,” *Phys. Rev. D* **88**, 054507 (2013), arXiv:1304.0483 [hep-ph].
- [119] B. Renner, “Empirical test of tensor meson dominance,” *Phys. Lett. B* **33**, 599–600 (1970).
- [120] K. Goeke, J. Grabis, J. Ossmann, P. Schweitzer, A. Silva, and D. Urbano, “The pion mass dependence of the nucleon form-factors of the energy momentum tensor in the chiral quark-soliton model,” *Phys. Rev. C* **75**, 055207 (2007), arXiv:hep-ph/0702031.
- [121] W. Broniowski, E. Ruiz Arriola, and K. Golec-Biernat, “Generalized parton distributions of the pion in chiral quark models and their QCD evolution,” *Phys. Rev. D* **77**, 034023 (2008), arXiv:0712.1012.
- [122] Maxim V. Polyakov and Peter Schweitzer, “Forces inside hadrons: pressure, surface tension, mechanical radius, and all that,” *Int. J. Mod. Phys. A* **33**, 1830025 (2018), arXiv:1805.06596 [hep-ph].
- [123] Muhammad Goharipour, Fatemeh Irani, M. H. Amiri, H. Fatehi, Behnam Falahi, A. Moradi, and K. Azizi (MMGPDs), “Can we determine the exact size of the nucleon?: A comprehensive study of different radii,” (2025), arXiv:2503.08847 [hep-ph].
- [124] S. D. Drell and Tung-Mow Yan, “Connection of Elastic Electromagnetic Nucleon Form-Factors at Large Q^{*2} and Deep Inelastic Structure Functions Near Threshold,” *Phys. Rev. Lett.* **24**, 181–185 (1970).
- [125] Cédric Lorcé, Luca Mantovani, and Barbara Pasquini, “Spatial distribution of angular momentum inside the nucleon,” *Phys. Lett. B* **776**, 38–47 (2018), arXiv:1704.08557 [hep-ph].
- [126] G. A. Miller, M. Strikman, and C. Weiss, “Pion transverse charge density from timelike form factor data,” *Phys. Rev. D* **83**, 013006 (2011), arXiv:1011.1472 [hep-ph].
- [127] Gerald A. Miller, “Singular Charge Density at the Center of the Pion?” *Phys. Rev. C* **79**, 055204 (2009), arXiv:0901.1117 [nucl-th].
- [128] Enrique Ruiz Arriola, Pablo Sanchez-Puertas, and Christian Weiss, “Pion transverse charge density from e^+e^- annihilation data and logarithmic dispersion relations,” (2025), arXiv:2503.10465 [hep-ph].
- [129] Julia Yu. Panteleeva and Maxim V. Polyakov, “Forces inside the nucleon on the light front from 3D Breit frame force distributions: Abel tomography case,” *Phys. Rev. D* **104**, 014008 (2021), arXiv:2102.10902 [hep-ph].
- [130] Adam Freese and Gerald A. Miller, “Unified formalism for electromagnetic and gravitational probes: Densities,” *Phys. Rev. D* **105**, 014003 (2022), arXiv:2108.03301 [hep-ph].